Structural changes of silicoaluminophosphate materials during catalytic reactions

Dissertation for degree of Philosophiae Doctor

Mahsa Zokaie

Department of Chemistry
InGAP-Innovative Natural Gas Processes and Products

Faculty of Mathematics and Natural Sciences
UNIVERSITY OF OSLO

September 2012

Series of dissertations submitted to the
Faculty of Mathematics and Natural Sciences, University of Oslo
No. 1259

ISSN 1501-7710

Cover: Inger Sandved Anfinsen.
Printed in Norway: AIT Oslo AS.

Produced in co-operation with Akademika publishing.
The thesis is produced by Akademika publishing merely in connection with the thesis defence. Kindly direct all inquiries regarding the thesis to the copyright holder or the unit which grants the doctorate.

Preface

The work presented in this thesis was carried out from November 2007 to December 2011 at inGAP Centre for Research-Based Innovation, Department of Chemistry, University of Oslo and was financed by Norwegian Research Council (NFR). I would like to thank Prof. Unni Olsbye for choosing me to be part of her team at inGAP.

It is with immense gratitude that I acknowledge the great guidance, support, and kindness of my supervisor prof. Karl Petter Lillerud for his outstanding pedagogical skills and for giving me this great opportunity to work on this project.

My most heartfelt gratitude goes to my supervisor, Dr. Ole Swang. The enthusiasm and inspiration he provided, along with a great effort to explain everything in a simple and clear way, helped me enjoy working in atomic scale. Every meeting with him was full of encouragement, humor and lots of great ideas.

I am very grateful for the personal encouragement and academic insights of Dr. Merete Hellner Nilsen whose support has been invaluable from the day one of starting my Ph.D.

I also like to thank Terje Fuglerud and Arne Grønvold for great scientific discussions during my internship at INEOS Chlorvinyls that helped me to finally link the molecular understanding and industrial sized applications of catalysis.

I owe my sincere gratitude to my colleagues in catalysis group and inGAP for always being there whenever I had a question or needed help to unscrew an autoclave in lab, and most important for giving me the feeling that I am not alone in this journey. I also like to thank my officemate Madeleine Diskus and Francesca Lønstad Bleken, for being by my side through all the good times and the bad.

Special gratitude goes to my friend Atoosa for every little thing, every concern, every laugh, every motivation, and most of all for the great lunch time we had together. Also, I like to use this opportunity to thank my aunt and Kian for encouraging me to come to Norway for my Ph.D, for their love, care and letting me be part of their family. I would also like to express my great appreciation to my husband's family for their support and care.

Lastly, and most importantly, I wish to thank my family; my son Aiden, for being such a great company during the long months of writing and for his encouraging kicks when writing seemed to be endless. My husband, Reza, for all the inspiring and motivating conversations, for all the support and love that kept me going, for always believing in me

even when I didn't believe in myself. My sister Maryam, who is always a bright point in my heart and for her pure love and joy which is sorely missed in the family. To my parents for instilling in me the belief that I could do absolutely anything, for encouraging me to leave them to follow my dreams, although I know it has been so difficult for them to live so far from me and the most important for their endless love.

To them I dedicate this thesis.

Mahsa Zokaie
September 2012-Oslo

Table of Contents

List of publications

This thesis is mainly based on the following manuscripts and unpublished results which all are summarized in Chapter 4. The manuscripts are collected in the appendix. The contribution of the author in each manuscript is specified on page v.

Paper I: *A computational study on heteroatom distribution in zeotype materials*
Mahsa Zokaie, Unni Olsbye, Karl Petter Lillerud and Ole Swang

Microporous Mesoporous Mater.,2012, *158*, *175-179*

Paper II: *Stabilization of silicon islands in SAPOs by proton redistribution*
Mahsa Zokaie, Unni Olsbye, Karl Petter Lillerud and Ole Swang

J. Phys. Chem. C, 2012, 116 (13), 7255–7259

Paper III: *Unit cell expansion upon coke formation in a SAPO-34 catalyst: A combined experimental and computational study*
Mahsa Zokaie, David Wragg, Arne Grønvold, Terje Fuglerud, Jasmina Hafizovic Cavka, Karl Petter Lillerud and Ole Swang

Microporous Mesoporous Mater., 2013, *165*, *1-5*

Manuscript I: *Lumpy Gravy: Size Distribution of Silicon Islands in SAPO Materials Based on Atomistic Modeling*
Mahsa Zokaie, Unni Olsbye, Karl Petter Lillerud and Ole Swang

Unpublished results I: *Analysis of ^{29}Si NMR spectra for varieties of shapes and sizes of silicon islands*

Unpublished results II: S*ynthesis and characterization of SAPO-34 using N,N,N trimethyl-1-adamantammonium as a template*

Poster I: *CHA and SAPO-34: Lattice stability dependence on position of acid sites*

Mahsa Zokaie, Ole Swang, Stian Svelle, Merete Hellner Nilsen, Unni Olsbye and Karl Petter Lillerud

ABC-6, 6th world congress on Catalysis by Acids and Bases (10-14 May 2009, Genova, Italy)

Poster II: *Silicon islands in SAPO materials: Thermodynamic considerations from atomistic modelling*

Mahsa Zokaie, Merete Hellner Nilsen, Unni Olsbye, Karl Petter Lillerud and Ole Swang

16th International Zeolite Conference (4-9 July 2010, Sorrento, Italy)

Poster III: *Proton Redistribution in Silicon Island of SAPO Material*

Mahsa Zokaie, Merete Hellner Nilsen, Unni Olsbye, Karl Petter Lillerud and Ole Swang

5th International FEZA Conference (3-7 July 2011, Valencia, Spain)

The author's contribution

In Paper I, II, Manuscript I and unpublished results I, the author performed all calculations and analysis of the data. In Paper III, the author performed all experiments and calculations except for synthesis of the samples (performed by: Jasmina Hafizovic Cavka) and refinement of PXRD patterns (performed by: David Wragg). In unpublished results II, all experiments were done by the author except for FTIR measurements which were performed in the group of professor Bordiga in Turin. The author also contributed in writing and preparation of all manuscripts.

Scope

The methanol-to-olefin (MTO) process is an alternative technology that can supply ethene and propene from sources other than petroleum feedstock. A range of well-known technologies that convert methanol to hydrocarbons can already be found, all of which are based on innovative catalyst systems. So far, among the materials that have been investigated for MTO catalysis, SAPO-34 has proven to be the best catalyst [1].The suitability of a material as a catalyst is determined by its activity, selectivity, accessibility and stability. SAPO-34 is a suitable catalyst based on the first three of these characteristics. Although the functionality of the SAPO-34 catalyst has further been demonstrated by the commercialization of the MTO process based on this catalyst [2], but there is still room for improvement of the current catalysts. There are both challenges due to rapid deactivation due to coke blocking the channels of the catalyst during the catalytic cycle and irreversible changes caused by reorganization of silicon during the regeneration step.

Zeolitic catalyst with the CHA topology, like SAPO-34 and SSZ-13, are among the structurally most suited materials for fundamental studies, since this is one of the few topologies where all T-sites are structurally identical. This make this material particularly suited for theoretical approaches. In this study, we addressed the effect of structural changes, both local and average, on zeolitic catalysts with the CHA toplogy. Both the effect of overall composition by comparing the aluminosilicate and SAPO version of the same structure, distribution and reorganisation of the active site are addressed as well as host guest interaction exemplified by calculations on lattice strain response to coke formation and synthesis of SAPO-34 with a new geometrically suited template.

Molecular mechanics methods have been the main method to achieve our goal, as they are well developed and have been applied in many promising studies to date. We were therefore able to focus our efforts on the chemistry of the material itself rather than developing new computational

methods. In some parts of the study, experimental investigations were used to provide supplementary information to our theoretical calculations. Experimental studies comparing the different CHA type catalysts have recently been performed by other members of the Catalysis group. The calculations in this work are motivated by a urge to gain a deeper understanding of these results.

The following three chapters, entitled Introduction, Experimental and Computational Methods, present the background for present work as well as the methods that were used during the study. The last chapter summarizes the results from the study and presents the conclusions.

1

1. Introduction

1.1. Zeolite and silicoaluminophosphate (SAPO) materials

Zeolites are a class of crystalline microporous materials made up of [SiO_4] or [AlO_4] tetrahedra, which by oxygen corner sharing atoms make a three dimensional framework. These tetrahedra are the primary building blocks of the framework. The extended arrangements of linked tetrahedra with [Si-O-Si] or [Si-O-Al] sequence may be defined as secondary building units (SBUs), like three-rings, four-rings, six-rings and more complex units like double-four-rings and double-six-rings. Various combinations of SBUs create numerous framework types of different geometries, sizes and pore connectivities [3].

Aluminophosphates (AlPOs) are another class of microporous materials with tetrahedra of [AlO_4] and [PO_4] [4]. The structure of this class of materials is similar to that of zeolites but with SBUs made of a [Al-O-P] link. The alteration between Al and P restrict the structural freedom to SBUs with an even number of T-atoms and do also introduce a larger charge distribution in the neutral framework. The introduction of silicon atoms into the neutral framework of AlPOs results in a new class of materials, called silicoaluminophosphates (SAPOs).

Three different mechanisms have been proposed for silicon substitution into the AlPO framework (Figure 1.1) [5]. The first mechanism, SM1, consists of the substitution of an aluminium atom by silicon. The second mechanism, SM2, is a silicon substitution for phosphorous. The proton

necessary to balance the charge of the framework (due to the Si substitution (+IV) for phosphorous (+V)) generates a surface bridge hydroxyl group that is known as a Brønsted acid site. The last mechanism is the simultaneous replacement of a pair of aluminium-phosphorous by two silicon atoms [6]. The SM1 mechanism is unlikely to happen as it leads to both a positive framework charge and the formation of a [Si-O-P] link that is known to be unstable [5, 7]. The combination of the SM2 and SM3 mechanisms leads to the formation of silicon aggregates or "silicon islands" [8]. Silicon islands are formed when at least two adjacent T sites are occupied by silicon [9, 10],[11].

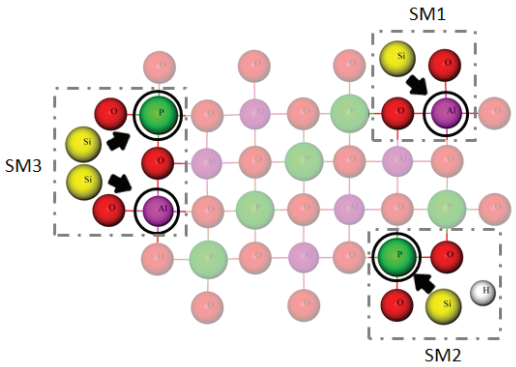

Figure 1.1. *A planar schematic of silicon incorporation mechanisms in an AlPO framework.*

1.2. Silicon island formation in SAPOs

One important feature of SAPO materials is the aggregation of silicon atoms to form so-called silicon islands (Figure 1.2). It is believed that silicon islands form when the silicon content reaches a threshold that is specific for each topology [12, 13]. To determine the threshold amount of isolated heteroatoms in different topologies, Barthomeuf *et al*. [14] studied the maximum content of isolated heteroatoms in different topologies of zeolites and zeotypes (SAPOs) using topological density[1]. They suggested that a higher number of isolated heteroatoms can be introduced into structures with lower topological density, based on topological constraints. The topological approach was later supported by Sastre *et al.* [6] who studied the topic theoretically. While silicon island

[1] Topological density ($TD_{2\text{-}5}$) is defined as $TD_{2-5} = \frac{\sum no.of\ tetrahedra\ in\ layer\ 2-5}{480}$ when $480 = \sum maximum\ theoritical\ no.of\ tetrahedra\ in\ layers\ 2-5$

formation is found to be thermodynamically favoured [10], there are few details about how such islands form. It seems that the aggregation of silicon into islands occurs due to migration of silicon T-atoms in the presence of vacancies and is promoted by extra framework spices like water [9, 15]. The formation of silicon islands may occur during synthesis or in post-synthesis modifications, such as calcination, which occur at high temperatures. As-synthesized islands occur in the samples where the silicon concentration in the synthesis gel is relatively high. Post-synthesis island formation occurs even in samples that lack islands in the as-synthesized sample [16].

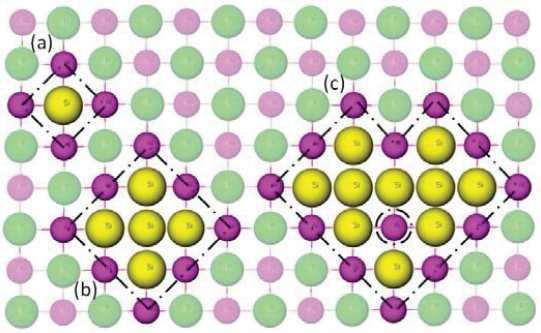

Figure 1.2. *Planar scheme of SAPO network: (a) isolated Si, (b) 5Si island, (c) silicon island with 1 Al inside the island [17].*

^{29}Si NMR of SAPOs gives us information about the identity of Al or Si for the atoms in the second coordination of tetrahedra around a central Si atom (Figure 1.3) and has therefore been an important tool in studying the aggregation of silicon atoms experimentally [13, 18-22]. Unfortunately it does not give precise information on size and shape of silicon islands, as many different silicon islands may be assigned to same NMR spectra.

Buchholz *et al*. [9] used a combination of chemical shifts in ^{29}Si NMR and x-ray diffraction to study silicon island formation upon heating. They observed that as silicon atoms aggregated (according to NMR), the crystallinity of the structures remained unchanged. This indicates that silicon atoms migration and vacant sites left by silicon do not impose any crystallinity changes on the framework that are detectable by x-ray diffraction, and therefore silicon vacant sites are somehow filled to avoid crystallinity loss. According to ^{31}P MAS NMR spectra, the migration of phosphorus atoms to silicon vacancies and their transformation from $P(OAl)_x(H_2O)_y$ to $P(OAl)_4$ species seems to

be the reason for the lack of changes in crystallinity during silicon island formation, a phenomenon known as structural healing [9].

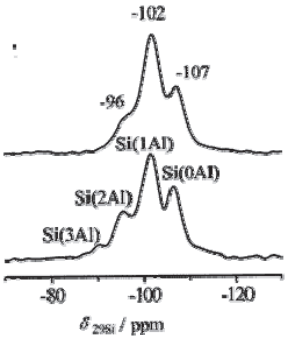

Figure 1.3 *^{29}Si NMR spectra for SAPO-34 [23].*

Another experimental method to study silicon islands was proposed by Martins *et al.* [24] who used a multipeak curve-fitting approach to analyse FTIR spectra in the OH stretching region of SAPO-34. Their analysis suggests the presence of three distinct acid sites (named OH_A, OH_B, and OH_C in Figure1.4). The components OH_A and OH_C have been assigned to proton attached oxygen atoms of different crystallographic positions in agreement with previous studies [24-27], while the OH_B sites had stronger acidity, as is expected in SAPOs. These were explained as protons at the borders of silica patches/islands, which can be used to identify the formation of silicon islands in the sample.

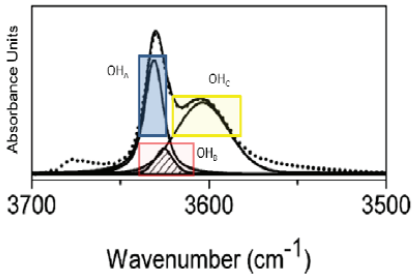

Figure 1.4. *FTIR spectra in the region of SAPO-34 samples [24].*

1.3. Acidity in SAPOs

Brønsted acidity in SAPOs is attributed to silicon incorporation in the framework while it is caused by aluminium in zeolites (Figure 1.5). Although the local structure of Brønsted acid sites is similar in SAPOs and zeolites (Si-O (H)-Al units), SAPOs are known to have milder acidity than zeolites, even when topologies and acid densities are similar [28, 29]. The acidity depends on several

factors: the bond angle, the bond length, the electrostatic potential around the acid centres and the first coordination sphere of T-atoms around the acid centres [30].

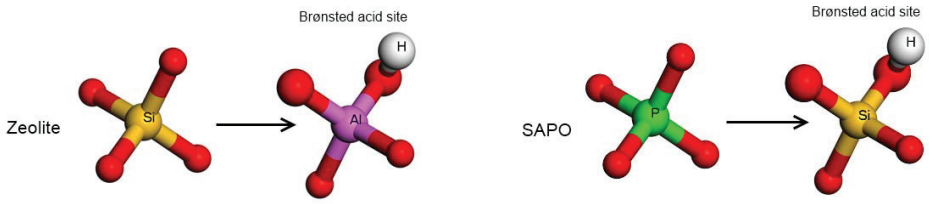

Figure 1.5. *Brønsted acidity in Zeolite and SAPO*

There are other types of acidity in SAPOs beyond that caused by bridging hydroxyl groups that come to the AlPO framework from silicon incorporation. Surface acidity in SAPOs may also result from protonic (Brønsted) sites or aprotonic (Lewis) sites.

1.3.1. Brønsted acidity

Brønsted acidity could potentially arise from hydroxyl groups, classified as:

a) Lattice termination silanol groups (Si-OH), aluminol (Al-OH) and P-OH [31, 32]

b) OH groups occurring at vacancy defect sites (hydroxyl nests) [33]

c) OH group attached to extra framework species

d) Bridging OH groups ($\equiv Si(OH)Al \equiv$) [32]

Of the groups mentioned above, only the last is acidic enough to be significant. The bridging OH group is usually what is meant when Brønsted acid sites are mentioned in SAPOs [34]. The formation of silicon islands has a direct impact on the acidity of SAPO materials. As a consequence of silicon island formation, the number of acid sites decreases and stronger acid sites (comparable with acid strength in zeolite) form at the border of the island [35, 36] or inside the island if it is large enough to house isolated Al-atoms, illustrated in figure 1.2c. A large silicon island is like a nano-zeollitic domain inside the SAPO.

1.3.2. Lewis acidity

Lewis acidity is another form of acidity in SAPOs that is derived from sites, accepting pairs of electrons. The source of Lewis acidity in SAPOs results from tri-coordinated Al sites on the framework and the extra lattice (non framework) Al sites [31]. The Lewis sites can be generated during high temperature treatments or during post-synthesis modification (i.e. silanation) [37]. Experiments show a correlation between crystallinity loss and the number of Lewis sites in a sample [38].

1.4. The CHA topology

The secondary building units (SBUs) of chabazite are 4-membered rings, 6-membered rings and double-6-rings [39]. The chabazite framework structure can then be described as chains of 4-rings, an AABBCC sequence of 6-membered rings or an ABC packing of double 6-rings. The resulting framework is characterized by a three-dimensional system confined by 8-membered rings and channel intersections, which are described as a cage [40]. Each cage in chabazite is bounded by 36 T-atoms, and every T-atom is shared by 3 cages (Figure 1.6).

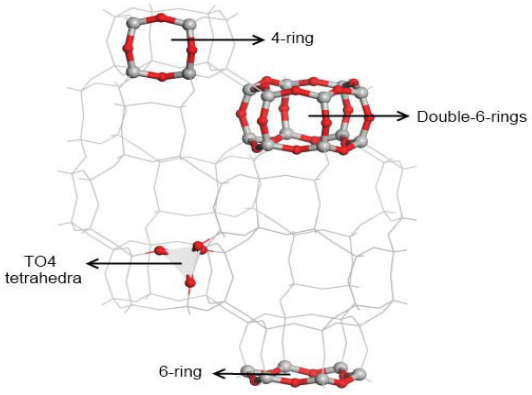

Figure 1.6. *Chabazite (CHA) structure. The primary (TO_4 – tetrahedra) and secondary building units of chabazite (4-ring, 6-ring, Double-6-rings) are shown as coloured balls. Two cages are shown in the structure (Cage dimension and pore opening).*

The structure can be described either with a rhombohedra unitcell, containing 12 T-atoms and with idealized cell constants a=9.42 Å α=94.2 ^{o}, or in the three times larger hexagonal unit-cell containing 36 T-atoms and with idealized cell constants a=13.7 Å c=14.8 Å,

The symmetry for the topology is R-3m. In the chabazite topology there is only one symmetrically independent tetrahedral site (T-site) and four unique oxygen sites (Figure 1.7, which takes its labelling scheme from a report on the crystallographic structure of SAPO [41]). Therefore the protons introduced to ensure charge neutrality after silicon inclusion in AlPO-34 may coordinate with one of the four different oxygen atoms. The preferred position of the proton at isolated acid sites has been the subject of both experimental [24, 25, 27, 42-44] and computational [28, 45-48] studies. According to FTIR studies, two sites of differing acidity have been found, which can be interpreted in terms of the locality of the proton at different oxygen sites [24-27].

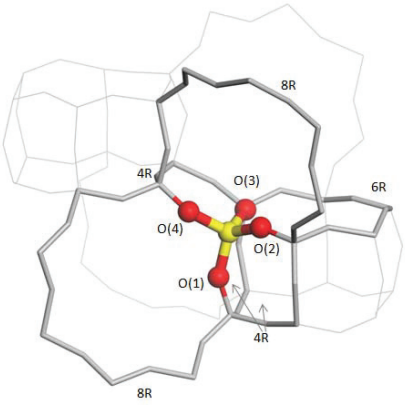

Figure1.7. *SAPO-34 structure with four different crystallographic oxygen atoms. Each oxygen atom is shared between : O(1) 2 4-member ring(MR) and 1 8-MR, O(2) 1 4-MR, 6-MR and 8-MR, O(3) 2 4-MR and 1 6-MR and O(4) 1 4-MR and 2 8-MR.*

1.4.1 SAPO-34

SAPO-34, a silicoaluminophosphate with chabazite topology, has been the main focus in all the theoretical and experimental work done in this study. A brief review of its application and synthesis conditions is therefore provided in the following section.

1.4.1.1 Applications

The most important application for SAPO-34 is a catalyst in conversion of methanol to light olefins (MTO) [49, 50] which is a process that recently has been commercialized. SAPO-34 may also find application in the conversion of methyl halide to light olefins [51-53]and in the removal of NO_x from diesel vehicles [54] as well as membrane applications in carbon dioxide-methane separation in natural gas processing [55].

Catalyst in methanol-to-olefins (MTO) conversion

Ethene and propene are the building blocks for the production of many synthetic hydrocarbons such as plastics, fibres and other chemical intermediates. They are by far the two largest products by volume produced by the petrochemical industry, which are mainly (60%) consumed in polyethene and polypropene production. Ethene and propene are mainly produced by the steam cracking of naphtha or other hydrocarbons. However, steam cracking will not be able to cover the expected demand for olefin production in the coming decades. Methanol is an alternative source for the production of light olefins and since it is mainly produced from natural gas, it decreases the dependence of olefin production on petroleum feedstock. Further developments in methanol production from other sources such as biomass and coal make the methanol-to-olefin process even more interesting [56].

The conversion of methanol to olefins is possible thanks to shape-selective catalysts with Brønsted acidity such as ZSM-5 and SAPO-34. Shape selectivity is when the transformation of reactants into products depends on how the processed molecules fit the active sites of the catalyst. It may be expressed as: a) reactant shape selectivity, which is important in multi-component feeds where the active sites of the catalyst located in channels and cages of the structure are only accessible to molecules small enough to enter the pores; b) transition state shape selectivity, which inhibits the formation of bulky molecules that are too large to fit inside the cage, and; c) product shape

selectivity, where the diffusion of products over a certain size is prohibited, which means that only size-controlled olefins emerge from the catalyst (Figure 1.8) [57].

SAPO-34, which is categorized as having a small-pore structure, mainly produces ethene and propene, while ZSM-5 results in the significant production of C_5^+/ aromatics as by-products [58]. The weakness of SAPO-34 in its catalytic application is its relatively fast deactivation by the accumulation of large aromatics and the blockage of pores during the reaction [59-61]. This is a challenge for industry [2, 62], and requires expensive regeneration cycles after a predefined time on stream to counteract deactivation.

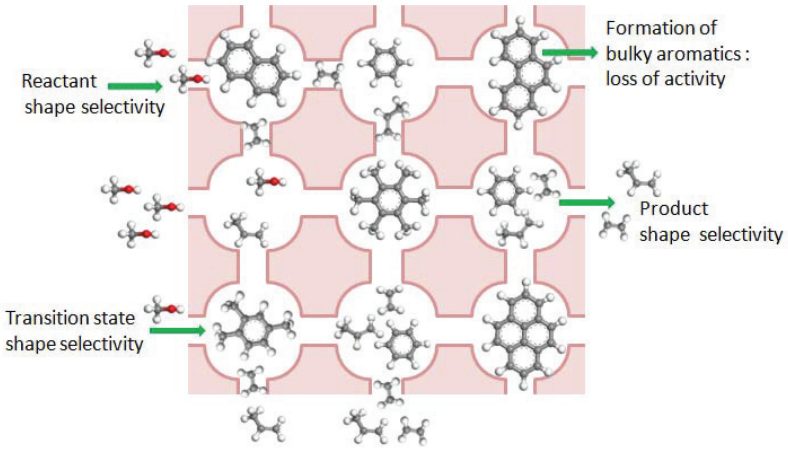

Figure 1.8. *Schematic of shape selectivity and loss of activity in SAPO-34 in methanol to olefins (MTO) conversion.*

1.4.2 SSZ-13

SSZ-13 is a high silica zeolite with the CHA topology patented by Chevron[63]. As mentioned in previous sections, an important application for materials that have CHA topology is as catalysts for the methanol-to-olefin (MTO) process, due to their shape selectivity. SSZ-13 shows a shape selectivity similar to SAPO-34, but the differences in chemical composition and milder Brønsted acidity makes SAPO-34 the preferred MTO catalyst. Comparative studies of the catalytic performance of SSZ-13 and SAPO-34 show that SAPO-34 catalysts are less prone to deactivation by coking than an SSZ-13 sample of equal acid site density. A comparison of the product selectivity

showed that SSZ-13 produced more coke and paraffins than SAPO-34 because of its stronger acid sites [64]. However, other investigations have shown that the temperatures for optimum conversion capacity [1] are 400 °C for H-SAPO-34 and 350–375 °C for H-SSZ-13[65]. At lower temperatures (300–350 °C), the conversion capacity of H-SSZ-13 was found to be even higher than of H-SAPO-34. This finding suggests that if we can improve the stability of SSZ-13 in coke formation, the MTO process might be operated at significantly lower temperatures, enabling significantly lower energy consumption [66].

1.5. SAPO-34 synthesis

Many parameters can be tuned in the synthesis of SAPO-34 (similar to other microporous materials) to affect the purity, crystallinity, defects and morphology of the crystals obtained. These parameters are:

a) Crystallization conditions: Temperature, static/stirring, seeding, gel ageing, microwave/conventional heating and length of induction period.

b) Composition-dependent parameters: alkalinity, dilution, the source and amount of each reactant, type and concentration of the organic molecules [67].

Hydrothermal synthesis of SAPO-34 is typically carried out at temperatures ranging from 443 to 473 K in an autoclave for 24–96 h. Obtaining a pure SAPO-34 phase can be very challenging since SAPO-5(AFI) [68], SAPO-18(AEI) [12] and AlPO-11(AEL) [69] are competing phases in the synthesis and appear as co-phases under a wide range of synthesis conditions. Conventional heating is usually preferred over microwave heating since using the latter yields SAPO-5 (AFI) as the main crystalline phase [70].

During preparation of the synthesis gel, an organic molecule is added to the mixture in order to ensure complete crystallization, increase the probability of producing the desired phase, balance the framework charge and fill voids in the framework [71]. Organic molecules, which are used as a template in synthesis, have a significant influence not only on the crystallinity of the framework but also on the properties, such as the silicon distribution in a SAPO material. Barthomeuf *et al.* [17] studied silicon island formation during the synthesis of SAPO materials and observed that silicon dispersity depends on the packing value of the template used during synthesis, that is, the number of

[1] Conversion capacity: total amount of converted methanol (gram) per catalyst weight (gram) before complete deactivation.

template molecules that can be accommodated by a single cavity. Smaller templates, such as morpholine, provide more positive charges to balance the negative charge caused by silicon incorporation in the network, which thus results in higher silicon dispersion. Gómez-Hortigüela *et al.* [15] suggested that differences in silicon incorporation are not derived from different packing values of the template, but by varying the number of water molecules located in the cavities in the structure to fill the space left over by the template. Furthermore, they suggested that more water molecules in the cavities leads to a greater dispersion of silicon atoms in the structure.

1.6. Defects in crystals

Perfect crystals have regular atomic arrangements that display translational symmetry. However, all crystalline materials have some degree of imperfection. The regular pattern of atoms may be interrupted by crystal defects, and certain properties of real crystals are determined by their defects. A defect in a solid is defined as any deviation from the perfectly ordered lattice structure [72]. Defects are categorized by their dimensionality into: a) *point defects* (0-dimensional), which are lattice distortions of the order of magnitude of atomic radii; b) *line defects* (1-dimensional), which define lines of lattice dislocations, and; c) *plane defect* (2-dimensional), which is a violation of translational symmetry along a surface with a thickness of an interatomic distance [73].

Point defects in a lattice may be of the vacancy, interstitial or substitutional type [74]. These types of point defects are schematically shown in Figure 1.9. If the defect is caused by an impurity then it is called an extrinsic defect; otherwise it is intrinsic. Based on this definition, vacancies are considered intrinsic defects, substitutional defects are considered extrinsic and interstitial defects may be intrinsic or extrinsic. Extrinsic defects are defects that can be controlled; they can be created by adding dopants to a system to create specific properties. In fact, many crystalline materials are interesting first and foremost because of their defects. This has been described as "perfecting imperfection" [75].

The substitution of silicon by aluminium in zeolites and phosphorous / aluminium by silicon in SAPO materials may, when the substitution is relatively low, be described as substitutional defects. As mentioned above, these defects are the source of Brønsted acidity in these materials, and thus are the source of their catalytic applications.

Substitutional defects in porous oxides have been studied extensively, while vacancies have attracted much less attention. Vacancies play an important role in the mobility of atoms and thereby formation of silicon islands which is one of the main topics in this thesis.

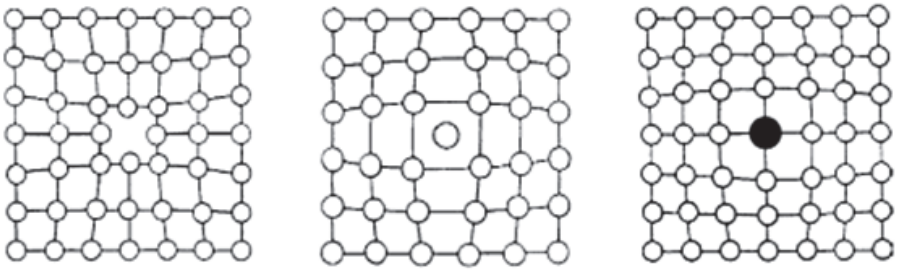

Figure 1.9. *Schematic of point defect types in crystalline materials. Left to right: Vacancy , interstitial and substitutional defects [74].*

2

2. Experimental methods

This chapter presents a general overview of the experimental methods and procedures used in this study. The text includes only methods that were employed by the author of this thesis.

2.1. Synthesis

In the course of this work, hydrothermal synthesis was used to synthesize SAPO-34. Hydrothermal synthesis is a term to describe a method to synthesize crystalline materials under high temperature and high pressure conditions, where water is the main solvent. In this type of synthesis, autoclaves made of an outer part of steel and an inner part of a Teflon liner are used as crystallization vessels.

We synthesized SAPO-34 with N,N,N trimethyl-1-adamantammonium (TMAda-OH) as the structure-directing agent (SDA). TMAda-OH was chosen since this ion fits geometrically tight in the cages of the CHA-structure (figure 2.1) and thereby stabilizes the structure due to Van der Waals interactions. This template has been used in the synthesis of the high silica chabazite materials SSZ-13 and SSZ-63 as well as the pure Si-chabazite. The elemental composition, local microscopic structure and morphology of SAPO-34 may change with the use of different SDAs. Therefore, the catalytic performance of the obtained materials made with tetramethylammonium hydroxide (TMAOH) and morpholine may be different. TMAda-OH, which is the geometrically most specific SDA, has, surprisingly, not been used for the synthesis of SAPO-34 in the literature.

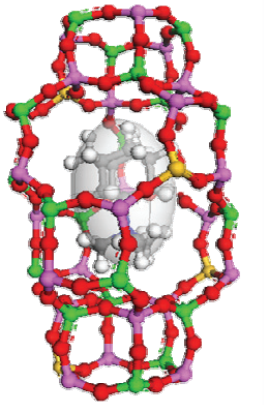

***Figure 2.1**. SAPO-34 and TMAda-OH inside the cage*

After preparation of a synthesis gel and the addition into the Teflon liner, it was sealed in the autoclave and transferred to a preheated oven for a predefined time. After crystallization, the as-synthesized sample was obtained by centrifugation, washing and drying in an oven overnight. Then, the as-synthesized sample was stored and characterized.

2.2. Characterization

2.2.1. Powder X-ray diffraction

Powder X-ray Diffraction (PXRD) is one of the primary techniques to characterize crystalline materials such as zeolites. In the PXRD technique, a powdered sample of the material is placed in a holder. The sample is then illuminated with x-rays of a fixed wavelength, and the intensity of the reflected radiation is recorded. The position, intensity, shape and width of the reflections give information about the sample. A diffraction pattern is the fingerprint of a crystalline phase and is used to identify mixture of phases in a sample [76, 77].

The diffraction patterns for routine characterization of the synthesized samples were recorded using a Siemens D-5000 with a primary Ge (111) monochromator and Bragg-Brentano geometry using Cu $K_{\alpha 1}$ radiation (λ = 1.5406 Å). The samples were finely ground and mounted in a plastic sample holder for measurement.

To gather diffraction patterns for Rietveld refinment, the patterns were collected on a Bruker D5000 diffractometer with Cu $K_{\alpha 1}$ radiation. The instrument was equipped with a Ge (111) monochromator and a Braun position sensitive detector. The samples were contained in 0.7 mm quartz glass capillaries mounted in Swagelok fittings. A hot air blower was used if the experiment required heating.

2.2.2. Scanning electron microscopy (SEM)

In scanning electron microscopy (SEM), a narrow electron beam line is focused over the sample surface. Electrons interact with the atoms that make up the sample, producing electron signals. Detectors analyse the yield of secondary and backscattered electrons as a function of the position of the primary beam. Different parts of the surface possess different contrast based on their orientation, shape and chemical composition. Heavier elements that scatter electrons more strongly appear brighter in the image generated from high energy backscattered electrons. Therefore SEM images give information about size, morphology and composition of the crystals. In this study, SEM analysis was performed using a FEI Quanta 200 FEG-ESEM, with both an Everhart-Thornley (SE) and a solid-state (BS) detector.

2.2.3. Energy-dispersive X-ray spectroscopy (EDS)

Energy-dispersive X-ray spectroscopy (EDS), usually integrated in SEM, is a method that provides information about the chemical composition of a selected point on the sample based on analysing of the energy to the emitted X-rays. In this study, EDS analysis was performed on a FEI Quanta 200 FEG-ESEM with EDS, with both an Everhart-Thornley and a solid-state detector.

2.2.4. Thermogravimetric analysis (TGA) and temperature programmed desorption (TPD)

Thermogravimetric analysis (TGA) is a technique in which changes in weight are monitored relative to change in temperature or time. Measurements are usually performed with a controlled temperature program in a controlled atmosphere. Measurements are used primarily to determine the composition of materials and to predict their thermal stability at temperatures up to 600 to 1500°C

(depending on the furnace and sample holders). The technique can be used to characterize materials that exhibit weight change due to decomposition, dehydration or reactions with the atmosphere, (normally oxidation) In paper III, we used TGA technique to measure the amount of coke (heavy hydrocarbons) trapped in cages of SAPO-34. To ensure oxidation of all coke products, samples were heated to 750 °C under air.

Another application of TGA, which we have used in 'unpublished result II', is in acidity measurements of the samples by means of temperature programmed desorption (TPD) of a basic adsorbate. This method is used to determine the quantity and strength of the acid sites on the surface of samples. TPD of ammonia is a widely used method for the characterization of site densities in solid acids due to its small molecular size, which allows it to penetrate into all pores of the solid as well as its basic nature, which makes it capable of titrating acid sites. In this study, samples were saturated with ammonia at 120°C, which was a temperature that minimized the physisorption of the ammonia. For desorption, samples were heated to 500 °C at a rate of 10 ºC/min under a nitrogen atmosphere [78].

TGA was performed and the surface acidity of samples was measured using a Mettler Toledo TGA / SDTA851^{e}.

2.2.5. Surface area measurements

Surface area measurements are based on the measurement of a monolayer physisorbed gas (an inert gas, such as Ar or N_2) on the surface of sample. In this study, N_2-physisorption was performed on a Belsorp-mini II instrument at -196 ^{0}C during which samples were kept in vacuum for 5 h at 300 ^{0}C. The surface area was determined using the BET method based on P/P_0 data in range of 0.01-0.15 [79]. Prior to the activation in the adsorbtion instrument, the samples were calcined first at 500 ^{o}C for 3 hours and for 30 minutes at 550 ^{o}C in a dry 20% O_2/N_2 atmosphere.

2.3. Catalytic testing and analysis of the deactivated material

The characterization of materials followed by the testing of samples for catalytic performance qualities such as reactivity (activity and selectivity) and stability (lifetime) allows us to gain deeper insights into the relationship between structure and catalytic properties.

Testing of the activated (calcined) catalyst on the methanol-to-olefin conversion was performed in a fixed bed glass reactor at a specified temperature. The methanol feed was obtained by a fixed flow of He gas through a methanol saturator kept in a constant-temperature water bath. The reaction products were analysed using an automatic injection gas chromatograph (GC) (Agilent 6890A GC with FID, equipped with a HP-plot Q capillary column (15 m, 0.320 mm i.d. (inner diameter), stationary phase thickness 20 μm)) connected directly to the reactor outlet by a heated transfer line. From the GC data, information on reactivity and stability of the material for the MTO reaction was obtained based on the effluent that left the catalyst bed.

The formation of bulky aromatic compounds leads to blockage of pores and the eventual deactivation of the catalyst [59-61]. Large aromatic molecules trapped inside the cages of the catalyst were analysed using dissolution procedures as described in the literature [80, 81]. Typically, 20 mg of the used catalyst was transferred to a screw-cap Teflon vial and dissolved using 1 ml of 15% HF. After 30 minutes, the catalyst framework was expected to be completely dissolved, and the organic phase was extracted with 1 ml of dichloromethane (CH_2Cl_2) with hexachloroethane (C_2Cl_6) as internal standard (The volume of the injection may vary each time, even with automatic injector. An internal standard, which is constant in all the chromatograms is needed to be able to compare different chromatograms). The extract was analysed using an Agilent 6890 N gas chromatograph connected to an Agilent 5793 mass selective detector equipped with a HP-5MS column (60 m, 0.25 mm i.d., stationary phase thickness 0.25 μm). The temperature of the oven was programmed to 50 to 300 °C with a heating rate of 10 °C min^{-1} (hold time = 3 min at 50 °C and 15 min at 300 °C). All spectra were normalized according to the internal standard and the compounds were identified by comparison with the mass spectral library of the NIST98 database and quantified based on their response factor obtained from a known concentration of a standard solution.

3

3. Computational methods

Theoretical methods provide powerful tools for studying zeolite and zeotype materials. They may offer complementary information to experiments and assist in the interpretation of the experimental observations. The theoretical methods used here are divided in two main categories, molecular mechanics and quantum mechanics. Molecular mechanics methods are characterized by high computational speeds compared to quantum mechanics methods, due to the simple mathematical formulation. We have mainly used molecular mechanics methods for calculations, due to its high speed and applicability for large systems of periodic structures, but we are also aware of the drawbacks of the methods in certain applications. In some cases, we validate the molecular mechanics calculations using quantum mechanics/density functional theory (DFT), while for some calculations we only used DFT calculations. The next sections present the basis for computational methods that we have used during the course of this work.

3.1. Molecular mechanics

Molecular mechanics methods (MM) do not explicitly consider electrons in the system but lump them with nuclei to form atoms. The potential energy of a collection of atoms can be defined for every set of positions. Molecular mechanics is based on classical mechanics. Each atom is considered to be a single particle that is spherical and has a defined polarizability and constant net charge (which is usually calibrated against quantum chemical results). In principle, the molecules' structure and potential energy can be calculated for any molecular or crystal structure. This is possible thanks to the Born-Oppenheimer approximation, which states that electronic and nuclear

motions can be uncoupled from one another (considered separately) and electrons can (almost) immediately adjust their positions to the new nuclear configuration when the nuclei move. A molecule in the molecular mechanics approach is treated as a collection of balls (atoms) that are linked together by springs (bonds) (ball and spring model). The potential energy functions of various structural features are used to describe these interactions between atoms. A combination of potential energy functions is known as a force field. Typical force fields include intramolecular terms for stretch energy (the energy function for stretching a bond between two atoms), bending energy (required energy for bending an angle formed by three atoms), torsional energy (due to twisting around bonds) and non-bonded interactions, which include electrostatic and Van der Waals interactions [82-84]. Therefore, the potential energy function is expressed as the following equation:

$$E = \sum E_{str} + \sum E_{bend} + \sum E_{torsion} + \sum E_{VdW} + \sum E_{electrostatic}$$

There are many varieties of force fields in existence; some of them use more sophisticated equations to reproduce accurate molecular behaviour by including "*cross terms*" to account for coupling between the terms listed above. Force fields are defined by a set of parameters for each type of atom, depending not only on the type of element but also on its chemical nature. The force field's parameters may be determined either by empirical methods or through quantum chemistry calculations [85].

To describe interactions between the atoms of ionic nature in zeolite and zeotype materials, the "*shell model potential*" may be used [86]. This model incorporates electronic polarizability by representing an ion as a charged core that contains all the mass of the ions linked by springs,with defined force constants, to a massless, charged shell. This potential has been used for most of the calculations reported here, in conjunction with the GULP program described below. The shell model potential is, however, tailored to zeotype materials and is not applicable to organic fragments in its present form. For the simulation of adsorbed molecules inside zeolite pores, we used the COMPASS (Condensed-phase Optimized Molecular Potentials for Atomistic Simulation Studies) force fields [87] which is a member of the consistent family of force fields and have parameters available for both zeolites and organic molecules. Forcite, a part of the Materials Studio 5.0 program system [88], was employed for the COMPASS-based calculations.

General utility lattice program (GULP)

In this study, we used the *General Utility Lattice Program* (*GULP*) code [89] to perform geometry optimization and lattice energy calculations on the zeolite/zeotype structures (without internal organic guest molecules). Lattice calculations in GULP are formulated based on the Born model [90], which is:

$$U_{i,j}(r) = \frac{Z_i Z_j e^2}{r} + A \exp\left(\frac{-r}{\rho_{ij}}\right) - \frac{C}{r^6}$$

Where, Z_i is the formal charge of atom i, and A, ρ and C are the adjustable potential parameters that determine the force field. In this approximation, the components of the lattice energy are decomposed into two classes of long- and short-range potentials. The former includes electrostatic interactions (the first term in equation 2) and the latter is described by the two-body Buckingham potential, which is composed of the short-range Pauli repulsion and dispersion terms. The summation of electrostatic energy in real space is conditional and, if truncated, will lead to errors. Therefore the Ewald method is used to evaluate the summation of electrostatic potentials. To compensate for ion polarizability, a shell model [86] is incorporated into the potential model.

Several force fields can be used with the GULP platform. We chose to use the *Catlow* force field [91, 92] , which presents a well validated set of parameters for silicates and aluminophosphates. The Catlow force field uses formal charges to describe Si, Al and P and oxygen-oxygen shell model potential for O.

3.2. Molecular docking simulations of the zeolite/guest system

Molecular docking simulation includes the study of sorption and diffusion of guest molecules inside or on the outer surface of the zeolite. It does not involve chemical changes (bond breaking/ making), but only physisorption of the guest molecule to zeolites. The pore topology of different zeolites often favours the adsorption of molecules at particular sites and the formation of intermediates with a specific size and shape during the catalytic process in the internal void space due to the electrostatic and steric[1] factors. Therefore, understanding the conformation and location of molecules in the framework is critical to gaining insight into the catalytic nature of the zeolites [83,

[1] These factors are introduced into simple versions of the collision theory of reactions to take care of the fact that the reaction probability depends on certain mutual orientations of the reactant molecules.

93]. Another important application of docking in a zeolite material is to check the compatibility of an organic molecule as a structure directing agent (SDA) of a framework by checking the non-bonded interaction energy as a measure of the efficacy of the organic molecule to make the desired framework [94-102].

During the course of this work, the Monte Carlo simulation method - as implemented in the Sorption module in the Materials Studio 5.0 program system [88] - has been used to investigate the conformation or docking of a guest molecule inside the zeolite.

Monte Carlo Method

Monte Carlo (MC) methods are based on the use of random numbers and probability statistics to investigate the configuration of structures. During each Monte Carlo cycle, random changes are made to the guest molecule's current position, orientation, and conformation, if flexible. The new state is then compared to its predecessor. If the energy is lower than the previous configuration, the displacement is accepted. Otherwise the probability of accepting an energy increase $E(s') - E(s) > 0$ is equal to $e^{\frac{-[E(s')-E(s)]}{kT}}$ which decreases exponentially with the energy difference. (k is the Boltzmann constant and T is the temperature)

An essential feature of the sampling method is that it allows the system to explore states that are higher in energy. Although this momentarily worsens the object function, the system is able to escape from local minima and search for better ones. At high temperatures, it is possible for many states to be accepted, while at low temperatures, the majority of these probabilistic moves will be rejected. The main objective of *Monte Carlo simulated annealing* is to avoid becoming trapped in local minima. In this method, the temperature is slowly decreased during the course of the simulation. Initially, when the temperature is high, large energy increases are acceptable, allowing the system to explore a broad range of structures. As the temperature decreases, steps that lead to an increase in energy are increasingly disfavoured, thereby steering the system to neighbouring states with a lower energy. Eventually, when the temperature is very low, the system is forced to evolve to a local minimum [84, 85], which one may hope is the actual global minimum.

3.3. Modelling of defects

As discussed in Section 1.6 above, zeolite materials usually include defects within the structure, such as vacancies and interstitials, and the migration of these defects is believed to play a critical role in the chemistry associated with the materials under study. In this section, we describe computational methods for the treatment of defects. There are two commonly used methods to calculate defect energies.

a) The super cell with periodic boundary conditions: This approach introduces a defect in the central primitive cell in a super cell, to which periodic boundary conditions are applied (each super cell is modelled separately and repeated infinitely in x,y,z directions). Using this approach gives control over the number of defects per unit cell and is well suited to modelling high concentrations of defects where significant defect-defect interactions are found [103]. The main difficulty with this approach is that, when a charged defect is present, the Ewald summation diverges. To avoid this, a uniform background charge may be added to compensate for the cell charge [104]. The super cell approach has been used throughout the present work.

b) The Mott-Littleton method: In this approach, the crystal is divided into an inner region I and outer region II; region I, which includes the defect and its surrounding atoms (typically from 100-500 atoms), can be fully relaxed using geometry optimization techniques. In Region IIa, atoms are kept in fixed positions, and region IIb is modelled as a dielectric continuum [105-107]. This method has been successfully used to model the defects within zeolites in the past [108, 109].

3.4. Quantum mechanical modelling

Quantum mechanical (QM) methods are based on approximate solutions of the electronic Schrödinger equation of a system. There are two main classes of approximation: *"ab initio"* methods and methods based on Density Functional Theory (DFT).

QM calculations for the description of solid state systems can also be classified according to the atomic scale model in use: i) the periodic model ; ii) the cluster model and iii) the embedded model [110]. In calculations based on the periodic model all the atoms in the unit cell are treated at the same level of theory. The computations can be demanding for unit cells with many atoms. A cluster model is a fragment cut out of the solid; it is essentially a molecule used as a model for the solid. An advantage of this approach is that higher levels of theory can be applied. In the embedded

model, a high level of theory is applied on a small cluster and the remaining part of unit cell is modelled using molecular mechanics (MM).

Computationally, the cheapest ab initio method is the Hartree-Fock (HF) approach, which is based on a simple approximation to the true many-body wave function. Hartree-Fock theory, by assuming a single-determinant form of the wave function, neglects the correlation between electrons. The electrons are subject to an average non-local potential arising from the other electrons which, for some purposes, may be a rather crude approximation [85]. Especially in the description of the bond breaking and formation involved in chemical reactions, the HF method may be insufficient [111]. Post Hartree-Fock methods are methods developed to improve the HF method by adding a description of electron correlation. These methods are potentially very accurate, but their poor scaling with system size limits their applications. Periodic ab initio calculations can be performed on small and high symmetric unit cell, like that of CHA, but even with such a unit cell, computation becomes expensive as the symmetry decreases [112]. Post HF methods are mostly used in the study of small molecules or cluster models. The choice of cluster is critical for the accuracy of calculations [113] and even with a suitable cluster there is the approximation made in neglecting the long-range structure [114]. However, cluster calculations can be used for studying reaction mechanisms that occur on local active sites, including, in some cases, interactions between sorbate molecules and solid materials [114].

Most of the contemporary quantum mechanical studies on zeolites apply DFT, where periodicity can be taken into account without excessive computational cost due to the application of plane wave basis sets [115]. The main advantage of DFT methods over HF are their efficiency and scaling behaviour [116] , although to improve the accuracy large basis sets and gradient-corrected functionals should be used which somewhat increases the computational time [114]. A reasonable compromise between accuracy and chemical efficiency must be found. DFT methods may fail in certain cases, including in systems in which long-range correlation effects are important (like transition states of radical reactions) and systems with low-lying excited states, causing near-degeneracy. In the present work, none of these conditions arise, and we feel confident that DFT is a valid approach.

In this work we used DFT calculations, mainly to validate molecular mechanics results, but also to calculate the acidity of the zeolite with the ammonia absorption energy as an index [117]. The size and simplicity of the SAPO-34 unit cell allowed us to use periodic models in our calculations.

Density Functional Theory (DFT)

Density Functional Theory (DFT) is a Quantum Mechanical method that is not based on optimization of the wave functions, but on optimization of the electron density. Using the electron density significantly reduces the cost of the calculation. Whereas instead of depending on all the spatial coordinates (3N) of all the electrons (N), the electron density is only a function of 3 coordinates (x, y, z on which the electron density depends) [84, 85]. The energy functional in the Kohn-Sham formulation of DFT is defined as:

$$E(\rho) = T_S(\rho) + J(\rho) + E_{Ne}(\rho) + E_{XC}(\rho)$$

Where

$T_S(\rho)$: kinetic energy

$J(\rho)$: Electron-electron Coulomb repulsion

$E_{Ne}(\rho)$: Electron-nuclei attraction

$E_{XC}(\rho)$: Exchange-correlation potential

The three first terms can be solved exactly, but the last one (exchange-correlation) has to be approximated. The difference between DFT methods is the choice of the functional form of the exchange-correlation energy.

In DFT calculations, $E_{XC}(\rho)$ may be approximated by the local density approximation (LDA) or generalized-gradient approximation (GGA). In LDA, $E_{XC}(\rho)$ is set equal to the exchange-correlation energy of an electron in a homogeneous electron gas of the same density. The LDA is often surprisingly accurate for systems with slowly varying charge densities, but it has a tendency to favour more homogeneous systems and over-binds molecules and solids [118]. An obvious approach to improving the LDA is to include gradient corrections by making a function of the density and its gradient, which is done in the the generalized-gradient approximation, GGA.

DFT calculations using non-local density functions (e. g. GGA) with medium-sized basis sets usually give comparable results to the simpler post-HF ab initio methods for describing the crystal structure of zeolites [113].

The Dmol^3 program [119], which applies numerical functions to atom-centred atomic basis sets, was used for all DFT calculations in this work as implemented in the Materials Studio program system [88]. We used the PW91 generalized gradient approximation (GGA) function [120], as it has

been shown to give reliable results for zeolites [121-124]. DNP and TNP basis sets have been employed.

4

4. Synopsis of results

More than 90 % of new commercial chemical processes are based on highly selective catalysts. A trend in the development of new catalysts for the 21 century is not only high efficiency but also excellent selectivity. Crystalline nanoporous catalysts with the combination of high density of active sites per gram catalyst and tuneable selectivity due to possibilities offered by manipulation of the internal surface are among the few candidate materials that can meet these requirements. One of the important processes based on selective catalysis is the methanol-to-olefin (MTO) process, which is an alternative technology to supply ethene and propene from sources other than petroleum feedstock. So far, among the materials that have been investigated for MTO catalysis, SAPO-34 has proven to be the best [1]. The suitability of a material as a catalyst is determined by its activity, selectivity, accessibility and stability. SAPO-34 is a potentially suitable catalyst based on these first three characteristics, but poses deactivation and stability issues because of rapid deactivation due coke formation and permanent changes in surface structure and composition during the regeneration cycle. To improve the stability of the catalyst, we need to understand how it works as a catalyst at an atomic scale. This topic has been the focus of the catalysis group at UiO. Recently more attention has been devoted to the long term stability of the catalyst. Progress in both computational techniques and materials characterization has enabled a better understanding of the relationship between catalyst structure and catalytic chemistry. In spite of these advances over the last decades, we still know relatively little about how to enhance the long term stability of these materials.

We have chosen SAPO-34 as our model material for this study, not only because of its application as the catalyst used in the industrial MTO process, but also because of its relatively simple crystallographic structure which makes it suitable for fundamental studies.

The stability of SAPO-34 as a catalyst is greatly affected by migration of heteroatoms (active sites) in the framework. We have chosen to apply atomic-scale modelling to approach this challenge with molecular mechanics (MM) because it is computationally highly efficient and allow us to investigate sufficiently large systems. When necessary, we also checked the reliability of the MM calculations using density functional theory (DFT).

This issue is the main objective in Paper 1, Paper 2, Preliminary manuscript 1 and Unpublished results 1. The computational study in Paper 1 is a continuation of previous NMR studies that had been done in our group. The rest of the studies will be followed by NMR measurements of SAPO-34 samples in collaboration with SINTEF and INEOS ChlorVinyls.

The migration of acid sites is not the only obstacle that affects the activity of SAPO-34. Formation of heavy coke molecules during the MTO reaction leads to the blockage of pores and consecutive deactivation. Wragg *et al.* [125] performed in-situ powder X-ray diffraction studies on SAPO-34 under MTO reaction conditions and observed unit cell changes in SAPO-34 during the progress of the reaction. They suggest that the formation of intermediates and aromatics in the cages cause the expansion of the unit cell. In order to find clues regarding the mechanism of cell expansion during MTO reaction, we have performed a multidisciplinary study using powder X-ray diffraction, retained hydrocarbon analysis, thermogravimetric analysis (TGA) and molecular mechanics on the coked samples. The results are presented in Paper 3.

At the outset, the present project focused on the synthesis of model materials to be used in characterization and catalytic testing. We aimed to synthesize SAPO-34 with a wide range of acidity (Si/(Al+P) ratio) with the help of N,N,N trimethyl-1-adamantammonium (TMAda-OH) as a template. This organic molecule had been used before to synthesize SSZ-13 (the zeolite analogue of SAPO-34) with a wide range of Al/Si ratios. The reason that we chose TMAda-OH for our synthesis was the fit between the structure of this template and chabazite topology, which makes synthesis of pure SAPO-34 samples with low and high acidity possible. Unfortunately TMAda-OH samples delivered for this project contained traces of Na^+ as an impurity. This ruined months of efforts in the laboratory. After identifying the problem (contaminated template) we received a commercially produced batch of TMAda-OH from Sachem Inc. With the pure template, we eventually succeed in synthesizing pure SAPO-34 with a range of Si/(Al+P). Because of the obstacle in the synthesis work, we focused instead on computational work which is therefore larger than originally planned. In the present work,

theoretical and experimental methods are combined to address structural changes in SAPO-34 during the MTO reaction.

This chapter presents synopses of the results of the above-mentioned studies. The details of each study are included in the appendix in the form of journal papers and preliminary manuscripts.

Paper I: A computational study on heteroatom distribution in zeotype materials

The objective of this contribution was to compare heteroatoms distribution (Si in SAPO-34 and Al in SSZ-13) in as-synthesized (or deactivated) catalyst with calcined (activated) catalyst during calcination/ regeneration cycles. The primary idea of this computational study started from experimental and theoretical research made by several independent groups that studied heteroatoms distribution using different techniques and found that distribution of Al sites is not random but controlled by electrostatic (i.e. the presence of SDA)[15, 17, 126-130]. According to previous studies heteroatoms distribution in as-synthesized material follows Dempsey's rule but the picture changes when water and template molecules are removed from the pores by calcination. In the latter case, the results indicate that Dempsey's rule is violated through the formation of next-nearest neighbour heteroatom pairs (NNNP) – Al-O-Si-O-Al linkages. Based on mentioned previous studies, we computationally studied redistribution of heteroatoms with and without presence of template by applying Molecular Mechanics methodology that Schröder and Sauer [131] used to study distribution of aluminium atoms in a high-silica faujasite framework. We also applied first-principles DFT calculations to evaluate the reliability of the Molecular Mechanics approach.

To model the two situations; as-synthesized and activated catalysts, the framework charge was compensated in two ways: In the model for *calcined*, a proton was added to one of the neighbouring oxygen atoms of each of the two heteroatoms. In the *as synthesized* material, the framework charge is balanced by template molecules. Hence, we model it without protons by adding an extra charge of +1 (per each heteroatom) equally distributed over all Si atoms in SSZ-13 and Al and P atoms in SAPO-34 (Note that this could also be taken to represent a catalyst deactivated by coke). For each situation (as-synthesized and activated) models were made which heteroatoms were located in different sites and relative stability of each structure was calculated as a function of inter-site separation using Molecular Mechanics.

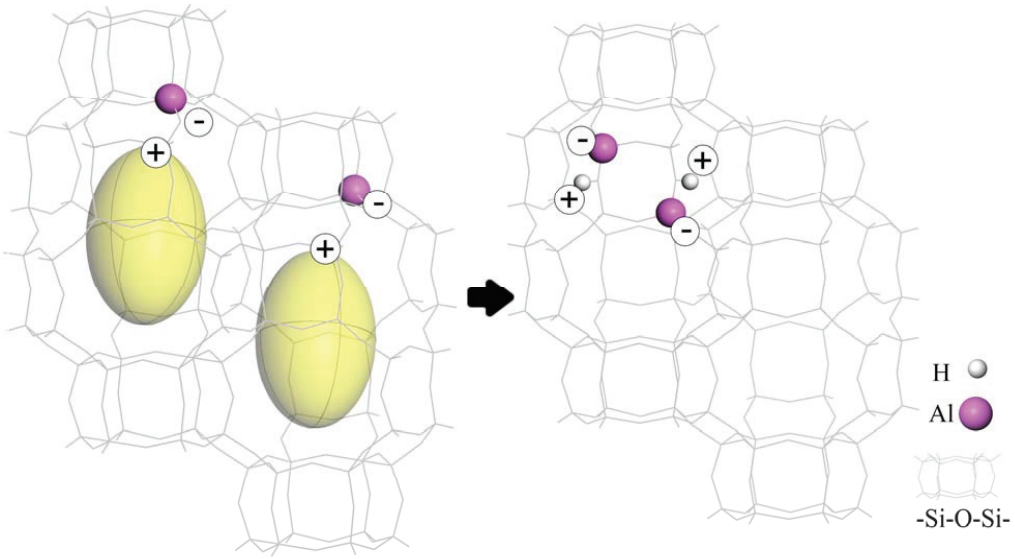

Figure 4.1. *Schematic representation of the calcination process for SSZ-13. a) As-synthesized SSZ-13; Illustration of a plausible distribution of aluminium sites in presence of SDA (adopted figure for SSZ-13 from article published by Shantz et al. [127]); aluminium sites are located nearby positively charged segment of SDA [127, 128] b) Calcined SSZ-13; As SDA is removed by calcination, aluminium atoms migrate in the framework to form Al-O-Si-O-Al linkage (NNNP configuration) [129].*

Relative energies as a function of interaluminium distance for as-synthesized SSZ-13 is plotted in Figure 4.2.a, showing a trend of stability increasing with inter-site separation. This is in agreement with experimental [127] and computational results[128]: Placement of aluminium sites in as-synthesized zeolites is controlled by template and aluminium sites which are located nearby positively charged segment of SDA (Figure 4.1.a). Figure 4.2.b shows lattice stability as a function of Al-Al distance for calcined SSZ-13. The first two points in the Figure correspond to aluminium atoms located in four-membered rings (4MR), containing an Al-O-Si-O-Al linkage (the NNNP configuration). Except for the stability of these two configurations, we do not see any clear trend in the energies as function of Al-Al separation.

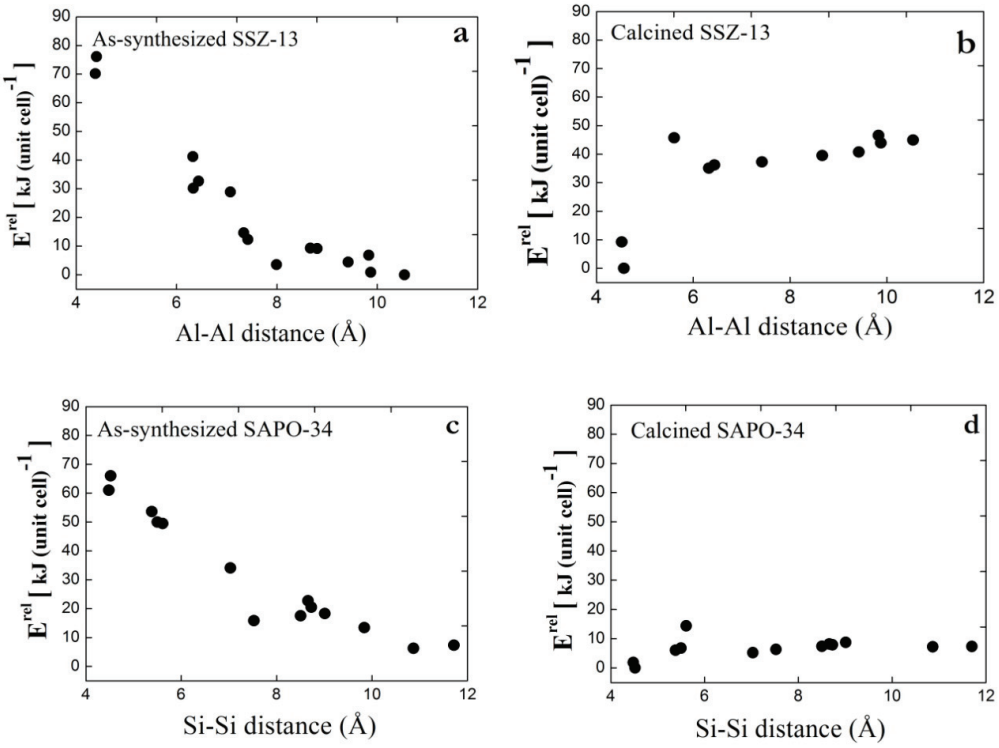

Figure 4.2 *Relative energy as a function of the heteroatoms distance in SSZ-13(a and b) and SAPO-34 (c and d) calculated by Molecular Mechanics. The framework charge(-2 per hexagonal cell) is compensated in : a and c) by protonation(active catalysts) ; b and d) by modifying all Si (b) or Al-P (d) charges (as-synthesized catalysts)*

Repeating the study for SAPO-34, we see the same tendency for as-synthesized SAPO-34 (Figure 4.2.c), but for calcined SAPO-34 (Figure 4.2.d) the tendency is much less pronounced compared to calcined SSZ-13. The NNNP configuration is stabilized by some 10 kJ/mol, in contrast to the roughly 40 kJ/mol seen in the case of SSZ-13. As a result, there is no strong tendency to form NNNP even at 300K.

To investigate the effect of close spacing between acid sites and their acidity, we calculated the acid strengths for different structures. There are several ways to evaluate the Brønsted acidity described in the literature, to wit: the calculations of proton affinity, partial atomic charge of the proton, the bonding energy between the acid site and different basic molecules[132, 133] and O-H stretch vibrational frequency [45, 134]. We chose to calculate the adsorption energies of ammonia at

the acid sites, because it is commonly used as a base probe in temperature-programmed desorption, an experimental method that we also used for characterizing the acidity of our samples in our experimental study.

Paper II: Stabilization of silicon islands in SAPOs by proton redistribution

This work is a theoretical study on proton re-distribution during the formation of silicon islands which is part of a bigger study on silicon island's shape and size. During the course of paper I, we found out that position of proton in SAPO-34, especially when the acid sites are close to each other, has very important impact on structure's stability. Therefore to study silicon island's growth and shape of the island, it was necessary to first study proton placement in silicon islands.

SAPO-34 has the highly symmetric chabazite topology with only one symmetrically independent tetrahedral site (T-site) and four unique oxygen sites (Figure 1.6). The protons introduced to ensure charge neutrality after silicon inclusion in $AlPO_4$ may coordinate to one of the four different oxygens. The preferred position of the proton at isolated acid sites has been the subject of both experimental [24, 25, 27, 42, 43] and computational [28, 45-48] studies. In earlier studies regarding silicon island in SAPO-34 [6, 45, 108], it was assumed that the protons, necessary to keep the silicon island neutral, would occupy the same positions as those preferred for solitary silicon atoms. Since it has been shown by experimental [135, 136] and theoritical [137-140] studies that protons in zeolite and zeotype material are mobile even at room temperature, we challenged the hypothesis, applied in previous works regarding the placement of protons in silicon island.

To study this, island of 5 silicon atoms was used as a model. Three protons that were needed to provide charge neutrality were located on different oxygen atoms (not inside the island [35]). Therefore we arrived at 108 different possible structures, only differing in the proton positions. Each of these structures was optimized using Molecular Mechanics.

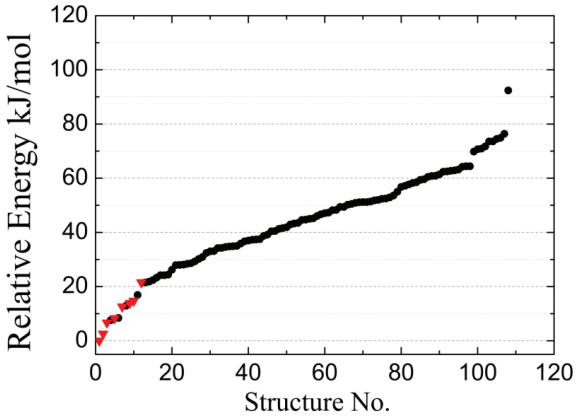

Figure 4.3. *Relative energies of different structures calculated by Molecular Mechanics. Black points are unstable structures and red points are remaining stable structures.*

The calculated relative energies for the 108 structures are plotted in Figure 4.3 (the most stable structure has been chosen as a zero energy reference). The results show that the proton placement is critical for stability. Careful analysis of the different structures yielded the following criteria for excluding structures as unstable:

a. Two protons connected to oxygen atoms in the same ring, disregarding ring size (4 ring, 6 ring and 8 ring).

b. All three protons connected to oxygen atoms connected to silicon atoms in the same double 6-ring.

c. At least one proton pointing towards large zeolite cavities or rings of larger than 8 T-atoms (Structures with proton on O(4)).

d. At least one proton connected to an oxygen atom in the O(2) positions.

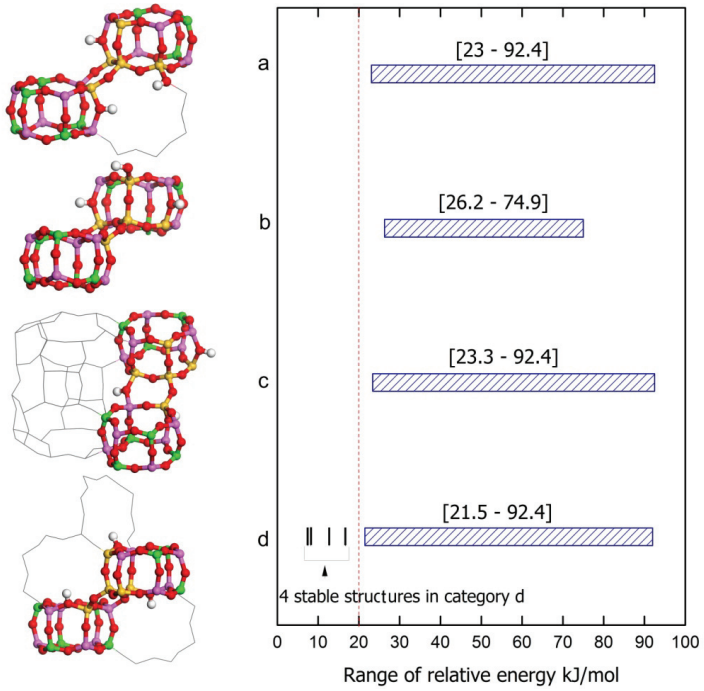

Figure 4.4. *Examples of unstable structures and their range of relative energies by Molecular Mechanics (MM) calculations. a) Protons connected to oxygen atoms in the same ring, b) Protons connected to tetrahedra located in the same double six ring, c) Proton pointing to open space (connected to O(4)) and d) Proton connected to O(2).*

Paper III: Unit cell expansion upon coke formation in SAPO-34 catalyst: A combined experimental and calculation study

In this work, combination of experimental and theoretical investigation was applied to study SAPO-34 cell expansion during the methanol-to-olefin (MTO) reaction. The primary idea of this study starts from work by Wragg *et al*. [125] who performed *in-situ* powder X-ray diffraction studies on SAPO-34 under reaction conditions and they observed unit cell changes in SAPO-34 with progress of the reaction. They suggested that formation of hydrocarbon-pool intermediates and aromatics in the cages cause expansion of the unit cell. In order to find clues regarding to the mechanism of cell expansion during MTO reaction, we thermally quenched the reaction after several

different times on stream. The coked samples were examined using X-ray diffraction (to establish unit cell dimensions), dissolution/extraction (to identify the organic residues; procedure of Magnoux et al. [81]) and thermogravimetric analysis (TGA; to determine total carbonaceous content). We then used Molecular Mechanics calculations (docking) to probe hydrocarbon molecules (found in the retained coke experiment) inside the cage and track the unit cell changes after formation of each of the molecules.

Docking's results reveal that hydrocarbons with one or two aromatic rings do not cause significant change in unit cell dimension. The considerable *c*-axis expansion and *a*- axis contraction only appears to start with the formation of bulky aromatics like phenanthrene. Refinement of X-ray diffraction suggest about 1% contraction in *a* and 3% expansion in *c*.

Analysis of the retained material shows that pyrene can be found in the framework as early as 30 minutes time-on-stream (TOS) which is in agreement with previous studies[141] and after 20 hours on-stream, when the *c*-axis expansion is more than 3%, less than half of the cages are filled with heavy coke molecules. Therefore, we investigated the hypothesis that one heavy coke molecule in a cage may affect the neighbouring cages and cause expansion in them. The hypothesis might be true due to the well-known flexibility of zeolite frameworks [142, 143].

To study the hypothesis, pyrene and phenanthrene were docked separately in the supercell of 24 hexagonal unit cells with different filling degree of cages. The expansion of the supercell was calculated in configurations where different numbers of cages were filled with pyrene / phenanthrene. The results are depicted in Figure 4.5. As soon as the first molecule is inserted, we see a sudden expansion of the whole structure, yet the insertion of more molecules leads to no further expansion. This finding explains why coked samples (like samples after 5 hr and 20 hr on stream) in which just a fraction of the cages are filled with heavy coke molecules show full expansion.

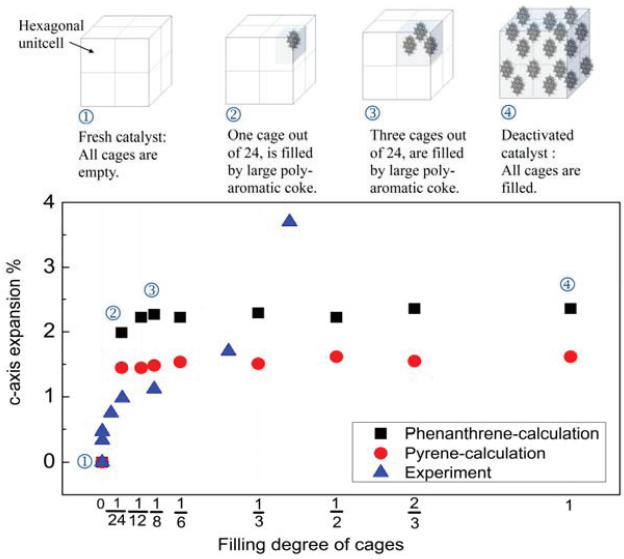

Figure 4.5. *Experimental and calculated c-axis expansion % vs. number of cages filled with bulky hydrocarbon molecules (calculations have been performed for phenanthrene and pyrene)*

This observation is supported by close analysis of the *in situ* PXRD data reported by Wragg et al [125]. The analysis of the (1 0 1) peak width at half maximum intensity (FWHM) presented in figure 9 of reference [125] shows a maximum value immediately after the initial expansion which is followed by a slight decline to a stable but slightly lower value of FWHM. This can be interpreted as a significant increase in microstrain as the initial expansion takes place, which is released slightly with time. A possible explanation for this is shown in cartoon form in Figure 4.6. As a few cages of the zeolite are filled with large coke molecules, the whole structure expands to accommodate this, resulting in significant strain, between filled and empty cages. As more of the cages fill up they become more equal in size and so the strain is released somewhat as the structure becomes more homogeneous.

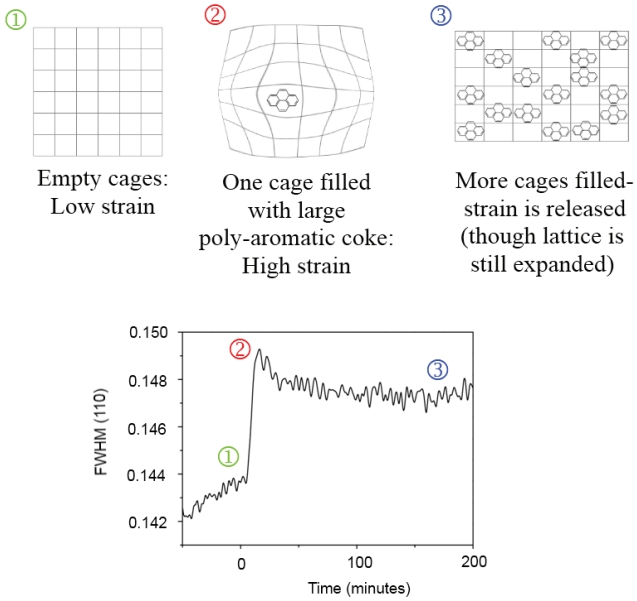

Figure 4.6. *a. Development and release of strain in the SAPO-34 structure due to partial and complete filling of cages with pyrene, b. Graph of FWHM from in situ PXRD data reproduced from data published in reference [125] .*

Manuscript I: Lumpy Gravy: Size Distribution of Silicon Islands in SAPO Materials Based on Atomistic Modeling (Preliminary)

In the present contribution, the optimum size of silicon islands in SAPO materials has been investigated along two different lines: A direct approach, where relative energies of models of different degrees of silicon agglomeration have been compared directly, and an indirect approach based on Ostwald ripening theory, in which we calculate critical radii from computed interfacial energies.

Direct calculation of island stabilities

In order to study the agglomeration of silicon atoms in SAPO materials and optimum size of the island, we calculate ground state energies of a SAPO system consisting of 8 hexagonal unit cells

containing 288 T-atoms of which 64 were silicon ($Si_{64}Al_{128}P_{96}O_{576}H_{32}$). Energies were computed for four different configurations of silicon islands (Figure 4.7):

a) 8 silicon islands of 8 atoms each

b) 4 silicon islands of 16 atoms each

c) 2 silicon islands of 32 atoms each

d) 1 silicon island of 64 atoms

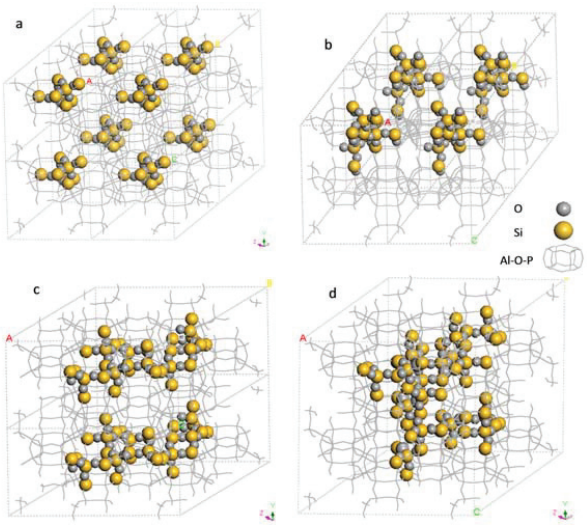

Figure 4.7. *The models for silicon islands of 64 silicon atoms: a- 8 silicon islands of 8 atoms each, b- 4 silicon islands of 16 atoms each, c- 2 silicon islands of 32 atoms each, d- 1 silicon island of 64 atoms.*

Relative energies as a function of island size are plotted in Table 4.1. We note that the curve does not go through a maximum – the energy increases monotonically. An interesting feature is the large energy gap seen between 16 and 32 T-atoms.

Table 4.1. *Relative energies (per mol unit cells) vs. number of silicon atoms in each island*

Number of silicon in each island	Relative energy kJ/unit cell
8	0
16	11.33
32	104.82
64	161.28

Calculation of critical radius of silicon island on the basis of interface energy

For the critical radius calculations, it has been assumed that silicon island formation can be viewed as an aggregation of a silica phase in form of sphere within the AlPO structure. In Ostwald ripening thermodynamics, free energy is given by the sum of two contributions:

$$G = -4/3\pi r^3 G_v + 4\pi r^2 \gamma \qquad (4.1)$$

Where, G_v is the bulk energy per unit volume and γ is the surface energy per unit area, assuming spherical particles. As the two energies have different signs, a balance is reached at a given critical radius r_c [144, 145].

$$r_c = 2\gamma / G_v \qquad (4.2)$$

Several models were developed to calculate the surface energy caused by the interaction between silicon islands and the aluminophosphate framework. In Figures 4.8, the different models are depicted, while surface and bulk energies and critical radii are shown in Figure 4.9 (as computed using Equations 4.1-2). Gratifyingly, the critical radii of different models are very similar, in the range of 7.4 to 7.9 Å.

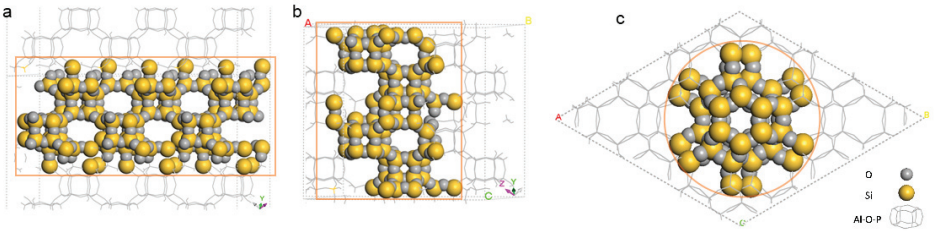

Figure 4.8. *Different models for surface energy calculation a) Horizontal slab model (SiO_2 and $AlPO_4$ phases as alternate slabs separated by planes in the (0 0 1) direction, b) Vertical slab model (SiO_2 and $AlPO_4$ phases as alternate slabs separated by planes in the (1 0 0) direction) and C) cylinder model (silicon island makes a cylinder within the $AlPO_4$ framework)*

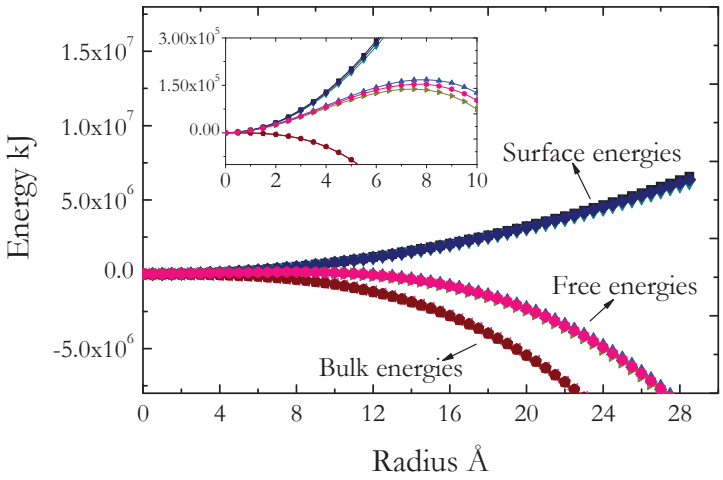

Figure 4.9. *Contributions to the free energy change associated with the silicon island formation due to Ostwald ripening. Inset plot is magnification of critical radii area to show the deviation of different models.*

Unpublished results I: Analysis of ^{29}Si NMR spectra for varieties of shapes and sizes of silicon islands

In this study we found all possible shapes of silicon islands in SAPO-34 which may give different ^{29}Si NMR spectra from size of 5 (the smallest stable island) to 16 silicon in island (the biggest possible from manuscript I). 16 silicon island were found with different shapes and sizes which corresponding Si(n-Al) neighbouring of each are reported in Table 4.2. The data is later going to be used in interpretation of ^{29}Si NMR spectra of SAPO-34.

Table 4.2. *All possible islands' shapes from 5-16 silicon atoms with corresponding Si(n-Al) neighbouring (to be compared to ^{29}Si NMR spectra)*

No. of silicon in island	Formula	Structure	Al-0	Al-1	Al-2	Al-3	Al-4
5	$Al^{3+} + 4P^{5+} \rightarrow 5Si^{4+} + 3H^{+}$	a	1	0	0	4	0
8	$2Al^{3+} + 6P^{5+} \rightarrow 8\ Si^{4+} + 4H^{+}$	b	2	0	2	4	0
9	$2Al^{3+} + 7P^{5+} \rightarrow 9Si^{4+} + 5H^{+}$	c	2	0	1	6	0
11	$3Al^{3+} + 8P^{5+} \rightarrow 11Si^{4+} + 6H^{+}$	d	3	1	2	5	0
12	$3Al^{3+} + 9P^{5+} \rightarrow 12Si^{4+} + 6H^{+}$	e	3	0	3	6	0
13	$3Al^{3+} + 10P^{5+} \rightarrow 13Si^{4+} + 7H^{+}$	f	3	0	1	9	0
14	$4Al^{3+} + 10P^{5+} \rightarrow 14Si^{4+} + 6H^{+}$	g	5	0	3	6	0
		h	4	0	6	4	0
		i	4	2	2	6	0
		j	4	0	4	6	0
15	$4Al^{3+} + 11P^{5+} \rightarrow 15Si^{4+} + 7H^{+}$	k	4	0	4	7	0
		l	4	2	1	8	0
		m	4	0	5	6	0
16	$4Al^{3+} + 12P^{5+} \rightarrow 16Si^{4+} + 8H^{+}$	n	4	1	2	9	0
		o	4	0	4	8	0
	$5Al^{3+} + 11P^{5+} \rightarrow 16\ Si^{4+} + 6H^{+}$		5	3	3	5	0

Unpublished results II: Synthesis and characterization of SAPO-34 using N,N,N trimethyl-1-adamantammonium as a template

In this contribution, SAPO-34 was synthesized using N,N,N trimethyl-1-adamantammonium (TMAda-OH) as template for the first time. Different parameters which affect phase crystallinity and purity, like gel composition, template concentration, crystallization time and temperature, were examined. The optimal composition for synthesis of SAPO-34 was found as follows (1–3)TMAda-OH: (0.2–0.8)SiO_2: 1.0Al_2O_3: 1.0 P_2O_5: 50H_2O. The samples were characterized using powder X-Ray diffraction, Scanning Electron Microscopy (SEM), NH_3-TGA, N_2-Physisorption measurement, FTIR spectroscopy with CO as probe molecule and catalytic testing.

Figure 4.10 shows X-ray diffraction patterns of as-synthesized samples. Peak positions and intensity match with the XRD pattern of pure SAPO-34 [41]. In Figure 4.11, SEM images of the as-synthesized material are shown. The morphology of the crystals is spheres made from layers not convectional cubic chabazite morphology.

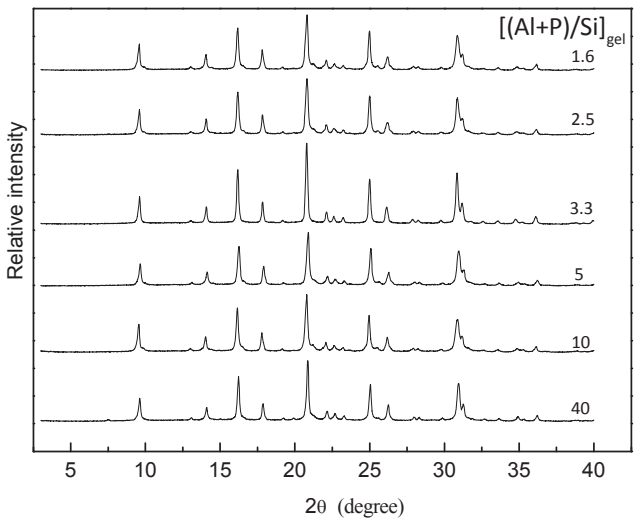

Figure 4.10. *XRD patterns of as-synthesized SAPO-34 samples*

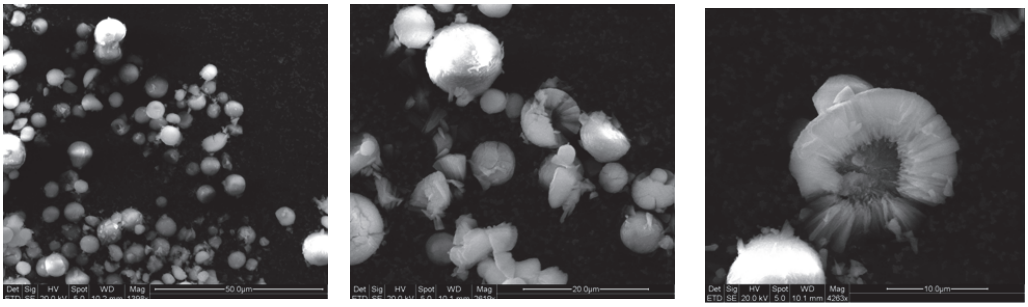

Figure 4.11 . *SEM images of as-synthesized samples*

4.1 Conclusions and suggestions for future work

This dissertation deals with structural changes that occur in SAPO-34 that affect its properties as an acidic catalyst. We also made SAPO-34 by using a new template that would provide more control over the amount of acid sites (Si/(Al+P) ratio) that are present in the framework.

Modelling of the silicon atom distribution and formation of silicon islands has been a subject of intense research during recent years. We have reviewed the literature concerning the issue and identified the main shortcomings of past research, and proposed new insights into the matter.

We were interested in investigating the migration of the heteroatoms (Al and Si atoms in SSZ-13 and SAPO-34 respectively) during the catalytic cycle. The formation of silicon islands in SAPO materials are the most visible evidence of the mobility of heteroatoms. This work has mainly focused on the stability of different configurations of heteroatoms. In the other words the driving force behind the reorganization of heteroatoms in zeolites and SAPOs.

This simple situation which is interaction between isolated heteroatoms in SSZ-13 and SAPO-34 can be studied as the starting point of silicon island formation in SAPO materials. We used molecular mechanics calculations of relative energies for different positions of two acid sites. Our calculations suggest that in the presence of protons (active catalyst), the most stable configuration are two acid sites separated by a single T-atom. The stability in the structure reduces by moving two active sites further. Removing the two acidic protons and distributing their charge evenly over all T-atoms to maintain neutrality (to mimic deactivated or as-synthesized catalyst) led to a change in the relative energies, and in this case the most stable configurations were those in which the inter-site distance was maximized. These results are in agreement with NMR studies that suggest that the mobility of acid sites during calcination in these materials is considerable. We also calculate the effect of inter-site distance of acid sites on the acidity using ammonia as a probe molecule. Our results suggest that the next-neighbour acid sites were less acidic than others, as should be expected since they represent structures of higher stability. These results corroborate earlier experimental studies that relied on measurements made using IR spectroscopy, NMR and neutron diffraction, in which two different acid strengths were found. Studies based on the above-mentioned methods suggest that at least two sites are of differing acidity, which was interpreted in terms of locality of single acid sites on different oxygen sites. In contrast, previous computational studies suggest that the four different oxygen sites have an equal chance of being protonated at room temperature. However, we suggested that defects in the structure may give rise to some of the different acidities

encountered experimentally. The sites of diminished acidity that have been observed in the above-mentioned studies could be the next-neighbour acid sites.

In our next study, we conducted a systematic investigation of the position of protons in the smallest stable silicon island (five Si- atoms) in SAPO-34. The preferred position of the proton at isolated acid sites has been the subject of both experimental and computational studies. We hypothesized that the most stable configuration of protons around a silicon island may not be inferred from the most stable proton coordination for a single silicon atom. Surprisingly, there are more than 100 possible proton distributions, even for this smallest silicon island, and our calculations showed that the total energy depends strongly on the proton location (different positions than those preferred for solitary silicon). We therefore suggest that proton redistribution will accompany silicon aggregation and island formation. By careful analysis of the different structures, we have established criteria to predict the stability of the proton configuration around a five-atom silicon island.

Previous calculations of the acidities of acid sites at silicon islands have been performed on islands with proton distributions that are unstable according to our criteria. In this study, we also used ammonia adsorption as an acidity index to investigate the effect of proton distribution on acidity. We compared acidity of all three protons on two structures (differing in proton location). The results indicate that the acidic sites surrounding an island are less acidic for the more stable proton configurations. To the extent that our five-atom model is representative of silicon islands in general, this may suggest that previous studies have overestimated the acidity of silicon island acid sites in SAPOs.

After establishing the instability criteria of the proton configurations around silicon islands and getting an idea about the optimal proton placement around silicon islands, we focused on the silicon islands' optimum size and shape in our next study. The formation of silicon islands is one of the phenomena that causes long-term deactivation of SAPO catalysts. Since there is a correlation between a decrease in the number of protons and an increase in the number of silicon atoms in the island, it is interesting to estimate the optimum size of the silicon island when designing the catalytic reaction. In this study, we investigated the growth of the silicon island to check whether the aggregation of silicon atoms continues until the formation of a two-phase ($AlPO_4$-SiO_2) material or whether it stops when reaching a specific size. The stability of silicon islands in SAPO materials has been computed using two different approaches: a direct approach, in which energies of islands of different sizes were compared directly; and an indirect approach based on the Ostwald ripening formalism and computed surface energies for the island/AlPO interface. In the direct calculations, we found that islands of sizes up to 16 T-atoms are roughly equally stable, with an apparent local

minimum at around 8 or 10 atoms. 32 and 64 atom islands are much less stable, to the extent that the population of such islands will be negligible even at elevated temperatures (~1000K). Our attempt at computing the critical radius from surface energies using the Ostwald ripening formalism indicates that growing islands will go through a maximum energy as a function of size at around 25-30 T-atoms, at odds with the direct stability calculations. The Ostwald model assumes spherical particle shape and that the particle size may be regarded as a continuum. These assumptions do not hold for silicon islands whose shape is far from spherical, and whose size is so small that the atomic structure represents a major divergence from homogeneous continuity.

As the direct approach suggested that silicon islands with 32 and 64 T-atoms are far less stable than islands of 16 silicon, and that islands from 5 up to 16 silicon are likely to occur, we investigated all the possible shapes and sizes (by avoiding Si-O-P linkage) of silicon islands up to 16. We arrived at 16 different islands. This data was needed to interpret the complex NMR spectra of the SAPO-34 samples that had silicon islands.

As our main concern in this project was to inspect structural changes that were somehow related to activity loss of the SAPO material during the catalytic reactions, we also modelled the unit cell expansion of SAPO-34 during the MTO reaction to get a better understanding of catalyst deactivation. For this study we used data taken from experimental coke analysis. Based on our calculations of the cell expansion caused by each hydrocarbon product, we suggest that there is no link between the production of small hydrocarbons and cell expansion. The calculations indicate that only the more bulky coke molecules, such as phenanthrene and pyrene, cause cell expansion. The presence of traces of pyrene at very early stages of the reaction is in agreement with the early expansion of the unit cell. Our calculations show that presence of pyrene in one cage can cause expansion of a super cell of 24 cages.

In parallel with the calculations, we also synthesized SAPO-34 using N,N,N trimethyl-1-adamantammonium (TMAda-OH) as a novel template. We obtained a pure phase with a wide range of Si/(Al+P) ratios, even though the morphology of the crystals was not the conventional cubic morphology of SAPO-34. FTIR measurements of the samples conducted with Prof. Silvia Bordiga's group at the University of Turin showed that samples have high amount of defect sites (terminal Si-OH, Al-OH and P-OH) that might be due to termination at the surface caused by the layered morphology. Further characterization of the samples may be interesting but was beyond the scope of this project.

We believe that one of the most important results of the present work is the knowledge of the strong correlation between proton configuration around silicon islands and the stabilities of the

islands. This opens opportunities for studying relative stabilities of silicon islands. Another important result is how coking influences unit cell expansion of zeotype materials during catalytic reactions. Until now, the imperfect correlation between coke amount and expansion has been somewhat puzzling. Our hypothesis that very few, large, coke precursor molecules may cause most of the expansion may have resolved this question.

The results presented in this thesis may be built upon in several ways. One possibility is a straightforward extension of our approach, but it is also possible to combine the results of the thesis with other research areas. The following issues are the most important and interesting for further exploration:

In the work reported here, defect-free models (the only defect included in our AlPO models is silicon substitution) were used for calculations, since this simplifies both calculations and analyses. However, we know from experiments that zeolites, like dense oxides, contain defects. Defects in microporous oxides, other than substitution to create acidity, has received little attention. This is partly due to the fact that characterization is complicated. NMR investigations of pure siliceous chabazite [146] indicate that 5 to 10 % of the T-atoms are next to a defect site. These defects are probably vacancies. One possibility for future research is to use models that account for defects in the calculations. These models may better mimic the real situation. Exactly which defects should be included presents an interesting question, especially because so few defects have been well characterized, but silanol nests may offer a good starting point. A project that approaches the mechanism for formation of vacancies in zeolites and SAPOs has already been initiated in the catalysis group [147].

In this work, we have investigated silicon islands in static forms, so that a possible follow-up could be to study the mechanism of silicon island formation. The formation of these silicon islands must involve the movement of distances equivalent to several unit cells during every regeneration cycle. This rapid movement has to involve vacancies. Studying the migration barriers, transition states and pathways that connect heteroatoms within the structure would provide more insight into the nature of migration.

The dependence of the instability criterion on proton location has been developed for SAPO-34, which has chabazite topology. We assume that with slight modification, these novel rules are transferable to other topologies, although testing this was beyond the scope of this project. Accordingly, further work could be directed towards the evaluation of the defined criteria for other topologies.

The SAPO-34 samples that were synthesized in this project were different from conventional samples. Surprisingly they contained more defects compared to SAPO-34 made with TMA as the template. The topology was also rather strange but the shape of the crystals is a parameter that is very sensitive to the synthesis conditions. Further optimization of the synthesis and investigation of the samples was beyond the time frame of this project, but may be another interesting project in itself.

As mentioned earlier, we believe that the best results can be obtained by combining experiments and calculations. Therefore, performing ^{29}Si NMR measurements on a series of model materials (with/without silicon islands) may be helpful in determining trends in silicon island formation and growth in combination with atom-scale modelling.

Zeotype materials have been commercially and scientifically important for some 50 years. It is fascinating that so many questions remain unanswered. We believe that the field holds rich future opportunities for both science and industry.

References

[1] A. Corma, J. Cejka, S. Zones; Zeolites and catalysis. Wiley-VCH-Verl.: 2010.
[2] M. Stöcker; Microporous Mesoporous Mater. 1999**,** 29 (1-2), 3-48.
[3] H. van Bekkum, E. Flanigen, K. Jansen; Studies in Surface Science and Catalysis. Elsevier: 1991; Vol. 58, xiii-xiv.
[4] S. T. Wilson, B. M. Lok, C. A. Messina, T. R. Cannan, E. M. Flanigen; J. Am. Chem. Soc. 1982**,** 104 (4), 1146-1147.
[5] E. M. Flanigen, R. L. Patton, S. T. Wilson; Studies in Surface Science and Catalysis. Elsevier: 1988; Vol. 37, 13-27.
[6] G. Sastre, D. W. Lewis, C. R. A. Catlow; J. Phys. Chem. B 1997**,** 101 (27), 5249-5262.
[7] C. S. Blackwell, R. L. Patton; J. Phys. Chem. 1988**,** 92 (13), 3965-3970.
[8] J. A. Martens, M. Mertens, P. J. Grobet, P. A. Jacobs; Studies in Surface Science and Catalysis. Elsevier: 1988; Vol. 37, 97-105.
[9] A. Buchholz, W. Wang, M. Xu, A. Arnold, M. Hunger; Microporous Mesoporous Mater. 2002**,** 56 (3), 267-278.
[10] M. Derewinski, M. J. Peltre, M. Briend, D. Barthomeuf, P. P. Man; J. Chem. Soc., Faraday Trans. 1993**,** 89 (11), 1823-1828.
[11] G. Sastre, D. W. Lewis, C. R. A. Catlow; J. Mol. Catal. A: Chem. 1997**,** 119 (1-3), 349-356.
[12] L. Xu, A. Du, Y. Wei, Y. Wang, Z. Yu, Y. He, X. Zhang, Z. Liu; Microporous Mesoporous Mater. 2008**,** 115 (3), 332-337.
[13] A. M. Prakash, S. Unnikrishnan; J. Chem. Soc., Faraday Trans. 1994**,** 90 (15), 2291-2296.
[14] D. Barthomeuf; J. Phys. Chem. 1993**,** 97 (39), 10092-10096.
[15] L. Gómez-Hortigüela, C. Márquez-Álvarez, M. Grande-Casas, R. García, J. Pérez-Pariente; Microporous Mesoporous Mater. 2009**,** 121 (1-3), 129-137.
[16] M. J. Peltre, P. P. Man, M. Briend, M. Derewinski, D. Barthomeuf; Catal. Lett. 1992**,** 16 (1), 123-128.
[17] D. Barthomeuf; Zeolites 1994**,** 14 (6), 394-401.
[18] E. Lippmaa, M. Maegi, A. Samoson, G. Engelhardt, A. R. Grimmer; J. Am. Chem. Soc. 1980**,** 102 (15), 4889-4893.
[19] E. Lippmaa, M. Maegi, A. Samoson, M. Tarmak, G. Engelhardt; J. Am. Chem. Soc. 1981**,** 103 (17), 4992-4996.
[20] J. Klinowski; Colloids Surf. 1989**,** 36 (2), 133-154.
[21] K. Jacek; Anal. Chim. Acta 1993**,** 283 (3), 929-965.
[22] S. Ashtekar, S. V. V. Chilukuri, D. K. Chakrabarty; J. Phys. Chem. 1994**,** 98 (18), 4878-4883.
[23] J. Jiao, S. Altwasser, W. Wang, J. Weitkamp, M. Hunger; J. Phys. Chem. B 2004**,** 108 (38), 14305-14310.
[24] G. A. V. Martins, G. Berlier, S. Coluccia, H. O. Pastore, G. B. Superti, G. Gatti, L. Marchese; J. Phys. Chem. C 2006**,** 111 (1), 330-339.
[25] L. Regli, S. Bordiga, A. Zecchina, M. Bjørgen, K. P. Lillerud, A. Gamba, C. Colella, S. Coluccia; Studies in Surface Science and Catalysis. Elsevier: 2005; Vol. 155, 471-479.
[26] L. J. Smith, A. Davidson, A. K. Cheetham; Catal. Lett. 1997**,** 49 (3), 143-146.
[27] L. Smith, A. K. Cheetham, L. Marchese, J. M. Thomas, P. A. Wright, J. Chen, E. Gianotti; Catal. Lett. 1996**,** 41 (1), 13-16.
[28] R. Shah, J. D. Gale, M. C. Payne; Chem. Commun. 1997**,** (1), 131-132.
[29] S. Bordiga, L. Regli, C. Lamberti, A. Zecchina, M. Bjørgen, K. P. Lillerud; J. Phys. Chem. B 2005**,** 109 (16), 7724-7732.
[30] H. O. Pastore, S. Coluccia, L. Marchese; Annu. Rev. Mater. Sci. 2005**,** 35 (1), 351-395.

[31] D. Barthomeuf; Acidity and Basicity of Solids: Theory, Assessment and Utility. Kluwer Academic Publishers: 1994; Vol. 444, 375-390.
[32] A. Zecchina, C. Lamberti, S. Bordiga; Catal. Today 1998**,** 41 (1-3), 169-177.
[33] A. A. Sokol, C. R. A. Catlow, J. M. Garces, A. Kuperman; J. Phys.: Condens. Matter 2004**,** 16 (27), S2781-S2794.
[34] K. A. Carrado, S. M. Auerbach, P. K. Dutta; Handbook of Zeolite Science and Technology. Marcel Dekker Incorporated: 2003.
[35] M. Briend, M. Derewinski, A. Lamy, D. Barthomeuf; Studies in Surface Science and Catalysis. Elsevier: 1993; Vol. 75, 409-420.
[36] A. F. Ojo, J. Dwyer, J. Dewing, P. J. O'Malley, A. Nabhan; J. Chem. Soc., Faraday Trans. 1992**,** 88 (1), 105-112.
[37] F. D. P. Mees, P. V. Der Voort, P. Cool, L. R. M. Martens, M. J. G. Janssen, A. A. Verberckmoes, G. J. Kennedy, R. B. Hall, K. Wang, E. F. Vansant; J. Phys. Chem. B 2003**,** 107 (14), 3161-3167.
[38] V. Nieminen, N. Kumar, T. Heikkilä, E. Laine, J. Villegas, T. Salmi, D. Y. Murzin; Appl. Catal., A: Gen 2004**,** 259 (2), 227-234.
[39] C. Baerlocher, W. M. Meier, D. H. Olson; Atlas of Zeolite Framework Types. Elsevier: 2001.
[40] L. S. Dent, J. V. Smith; Nature 1958**,** 181 (4626), 1794-1796.
[41] M. Ito, Y. Shimoyama, Y. Saito, Y. Tsurita, M. Otake; Acta Crystallogr. Sect. C: Cryst. Struct. Commun. 1985**,** 41 (12), 1698-1700.
[42] S. Bordiga, L. Regli, D. Cocina, C. Lamberti, M. Bjørgen, K. P. Lillerud; J. Phys. Chem. B 2005**,** 109 (7), 2779-2784.
[43] L. Smith, A. K. Cheetham, R. E. Morris, L. Marchese, J. M. Thomas, P. A. Wright, J. Chen; Science 1996**,** 271 (5250), 799-802.
[44] L. M. Bull, A. K. Cheetham, P. D. Hopkins, B. M. Powell; J. Chem. Soc., Chem. Commun. 1993**,** (15), 1196-1198.
[45] G. Sastre, D. W. Lewis; J. Chem. Soc., Faraday Trans. 1998**,** 94 (19), 3049-3058.
[46] M. Brändle; J. Chem. Phys. 1998**,** 109 (23), 10379.
[47] P. Ugliengo, B. Civalleri, C. M. Zicovich-Wilson, R. Dovesi; Chem. Phys. Lett. 2000**,** 318 (1-3), 247-255.
[48] Y. Jeanvoine, J. G. Ángyán, G. Kresse, J. Hafner; J. Phys. Chem. B 1998**,** 102 (29), 5573-5580.
[49] J. Q. Chen, A. Bozzano, B. Glover, T. Fuglerud, S. Kvisle; Catal. Today 2005**,** 106 (1-4), 103-107.
[50] M. Popova, C. Minchev, V. Kanazirev; Appl. Catal., A: Gen 1998**,** 169 (2), 227-235.
[51] Y. Wei, D. Zhang, Z. Liu, B. L. Su; J. Catal. 2006**,** 238 (1), 46-57.
[52] Y. Wei, D. Zhang, Y. He, L. Xu, Y. Yang, B. L. Su, Z. Liu; Catal. Lett. 2007**,** 114 (1), 30-35.
[53] S. Svelle, S. Aravinthan, M. Bjørgen, K. P. Lillerud, S. Kolboe, I. M. Dahl, U. Olsbye; J. Catal. 2006**,** 241 (2), 243-254.
[54] Z. Liu, L. Tang, L. Chang, J. Wang, W. Bao; Chinese J. Catal. 2011**,** 32 (3-4), 546-554.
[55] S. Li, J. G. Martinek, J. L. Falconer, R. D. Noble, T. Q. Gardner; Ind. Eng. Chem. Res. 2005**,** 44 (9), 3220-3228.
[56] G. A. Olah, A. Goeppert, G. K. S. Prakash; Beyond oil and gas: the methanol economy. Wiley-VCH: 2006.
[57] B. Smit, T. L. M. Maesen; Nature 2008**,** 451 (7179), 671-678.
[58] J. F. Haw, W. Song, D. M. Marcus, J. B. Nicholas; Acc. Chem. Res. 2003**,** 36 (5), 317-326.
[59] U. Olsbye, M. Bjørgen, S. Svelle, K. P. Lillerud, S. Kolboe; Catal. Today 2005**,** 106 (1-4), 108-111.
[60] I. M. Dahl, S. Kolboe; Catal. Lett. 1993**,** 20 (3), 329-336.

[61] I. M. Dahl, S. Kolboe; Journal of Catalysis 1994**,** 149 (2), 458-464.
[62] G. Qi, Z. Xie, W. Yang, S. Zhong, H. Liu, C. Zhang, Q. Chen; Fuel Process. Technol. 2007**,** 88 (5), 437-441.
[63] S. I. Zones; U.S Patent 4544538, 1985.
[64] L.-T. Yuen, S. I. Zones, T. V. Harris, E. J. Gallegos, A. Auroux; Microporous Mater. 1994**,** 2 (2), 105-117.
[65] F. Bleken, M. Bjørgen, L. Palumbo, S. Bordiga, S. Svelle, K. P. Lillerud, U. Olsbye; Top. Catal. 2009**,** 52 (3), 218-228.
[66] L. Sommer, D. Mores, S. Svelle, M. Stöcker, B. M. Weckhuysen, U. Olsbye; Microporous Mesoporous Mater. 2010**,** 132 (3), 384-394.
[67] F. Di Renzo; Catal. Today 1998**,** 41 (1-3), 37-40.
[68] Y. J. Lee, S. C. Baek, K. W. Jun; Appl. Catal., A: Gen 2007**,** 329, 130-136.
[69] G. Liu, P. Tian, J. Li, D. Zhang, F. Zhou, Z. Liu; Microporous Mesoporous Mater. 2008**,** 111 (1-3), 143-149.
[70] S. H. Jhung, J. S. Chang, J. S. Hwang, S. E. Park; Microporous Mesoporous Mater. 2003**,** 64 (1-3), 33-39.
[71] M. E. Davis, R. F. Lobo; Chem. Mater. 1992**,** 4 (4), 756-768.
[72] A. E. Hughes, D. Pooley; Real Solids and Radiation. Wykeham Publications: 1975.
[73] W. Borchardt-Ott, R. O. Gould; Crystallography: An Introduction. Springer: 2011.
[74] A. M. Kosevich; The Crystal Lattice: Phonons, Solitons, Dislocations, Superlattices. John Wiley & Sons: 2006.
[75] L. Cademartiri, G. A. Ozin, J. M. Lehn; Concepts of Nanochemistry. Wiley-VCH: 2009.
[76] G. Ertl, H. Knözinger, F. Schüth, J. Weitkamp; Handbook of Heterogeneous Catalysis. John Wiley & Sons: 2008; Vol. 2.
[77] I. Chorkendorff, J. W. Niemantsverdriet; Concepts of modern catalysis and kinetics. Wiley-VCH: 2007.
[78] M. Niwa, N. Katada, K. Okumura; Characterization and Design of Zeolite Catalysts: Solid Acidity, Shape Selectivity and Loading Properties. Springer: 2010.
[79] S. Brunauer, P. H. Emmett, E. Teller; J. Am. Chem. Soc. 1938**,** 60 (2), 309-319.
[80] M. Bjørgen, S. Svelle, F. Joensen, J. Nerlov, S. Kolboe, F. Bonino, L. Palumbo, S. Bordiga, U. Olsbye; J. Catal. 2007**,** 249 (2), 195-207.
[81] P. Magnoux, P. Roger, C. Canaff, V. Fouche, N. S. Gnep, M. Guisnet; Studies in Surface Science and Catalysis. Elsevier: 1987; Vol. 34, 317-330.
[82] C. R. A. Catlow, R. G. Bell, B. Slater; Computer Modelling of Microporous Materials. Academic Press: London, 2004; 1-24.
[83] R. Catlow, R. Bell, F. Cora, B. Slater; Studies in Surface Science and Catalysis. Elsevier: 2007; Vol. 168, 659-700.
[84] F. Jensen; Introduction to computational chemistry. John Wiley & Sons: 2007.
[85] C. J. Cramer; Essentials of computational chemistry: theories and models. Wiley: 2004.
[86] B. G. Dick, Jr., A. W. Overhauser; Phys. Rev. 1958**,** 112 (1), 90.
[87] H. Sun; J. Phys. Chem. B 1998**,** 102 (38), 7338-7364.
[88] Materials Studio, Accelrys Inc.: San Diego, CA. (http://www.accelrys.com).
[89] J. D. Gale; J. Chem. Soc., Faraday T rans. 1997**,** 93 (4), 629-637.
[90] J. Fan; Multiscale Analysis of Deformation and Failure of Materials. John Wiley & Sons: 2011.
[91] K. P. Schröder, J. Sauer, M. Leslie, C. R. A. Catlow, J. M. Thomas; Chem. Phys. Lett. 1992**,** 188 (3-4), 320-325.
[92] J. D. Gale, N. J. Henson; J. Chem. Soc., Faraday Trans. 1994**,** 90 (20), 3175-3179.

[93] B. Smit; Computer Modelling of Microporous Materials. Academic Press: London, 2004; 25-47.
[94] R. G. Bell, D. W. Lewis, P. Voigt, C. M. Freeman, J. M. Thomas, C. R. A. Catlow; Studies in Surface Science and Catalysis. Elsevier: 1994; Vol. 84, 2075-2082.
[95] R. Millini; Catal. Today 1998**,** 41 (1-3), 41-51.
[96] F. Jousse, L. Leherte, D. P. Vercauteren; J. Mol. Catal. A: Chem. 1997**,** 119 (1-3), 165-176.
[97] A. R. George, C. R. A. Catlow, J. M. Thomas; Microporous Mater. 1997**,** 11 (3-4), 97-105.
[98] D. F. Plant, A. Simperler, R. G. Bell; J. Phys. Chem. B 2006**,** 110 (12), 6170-6178.
[99] V. V. Guliants, J. T. Mullhaupt, J. M. Newsam, A. M. Gorman, C. M. Freeman; Catal. Today 1999**,** 50 (3-4), 661-668.
[100] B. H. Toby, N. Khosrovani, C. B. Dartt, M. E. Davis, J. B. Parise; Microporous Mesoporous Mater. 2000**,** 39 (1-2), 77-89.
[101] M. Elanany, B. L. Su, D. P. Vercauteren; J. Mol. Catal. A: Chem. 2007**,** 270 (1-2), 295-301.
[102] C. S. Cundy, P. A. Cox; Microporous Mesoporous Mater. 2005**,** 82 (1-2), 1-78.
[103] http://projects.ivec.org/gulp/help/gulp_30_manual/gulpnode23.html.
[104] A. R. Leach; Molecular Modelling: Principles and Applications. Prentice Hall: 2001.
[105] R. W. Grimes, C. R. A. Catlow, A. L. Shluger; Quantum Mechanical Cluster Calculations in Solid State Studies. World Scientific: 1992.
[106] W. Hayes, A. M. Stoneham; Defects and Defect Processes in Nonmetallic Solids. Dover Publications: 2004.
[107] C. R. A. Catlow, R. G. Bell, J. D. Gale; J. Mater. Chem. 1994**,** 4 (6), 781-792.
[108] G. Sastre, D. W. Lewis, C. R. A. Catlow; J. Phys. Chem. 1996**,** 100 (16), 6722-6730.
[109] D. W. Lewis, C. R. A. Catlow, G. Sankar, S. W. Carr; J. Phys. Chem. 1995**,** 99 (8), 2377-2383.
[110] P. Nachtigall, J. Sauer; Studies in Surface Science and Catalysis. Elsevier: 2007; Vol. 168, 701-736.
[111] J. B. Nicholas; Top. Catal. 1997**,** 4 (1), 157-171.
[112] C. Zicovich-Wilson, R. Dovesi; J. Mol. Catal. A: Chem. 1997**,** 119 (1–3), 449-458.
[113] J. Limtrakul, D. Tantanak; J Mol. Struc-THEOCHEM 1995**,** 358 (1–3), 179-193.
[114] D. W. Lewis; Zeolites, Computer Modeling of. Elsevier: Oxford, 2001; 9863-9868.
[115] J. D. Gale; Computer Modelling of Microporous Materials. Academic Press: London, 2004; 129-164.
[116] C. Tuma, J. Sauer; Chem. Phys. Lett. 2004**,** 387 (4–6), 388-394.
[117] R. R. Pinto, P. Borges, M. A. N. D. A. Lemos, F. Lemos, J. C. Védrine, E. G. Derouane, F. R. Ribeiro; Appl. Catal., A: Gen 2005**,** 284 (1-2), 39-46.
[118] J. P. Perdew, A. Ruzsinszky, L. A. Constantin, J. Sun, G. b. I. Csonka; J. Chem. Theory Comput. 2009**,** 5 (4), 902-908.
[119] B. Delley; J. Chem. Phys. 1990**,** 92 (1), 508-517.
[120] J. P. Perdew, J. A. Chevary, S. H. Vosko, K. A. Jackson, M. R. Pederson, D. J. Singh, C. Fiolhais; Phys. Rev. B 1992**,** 46 (11), 6671.
[121] J. Kučera, P. Nachtigall; Microporous Mesoporous Mater. 2005**,** 85 (3), 279-283.
[122] A. V. Larin, A. A. Rybakov, G. M. Zhidomirov, A. Mace, A. Laaksonen, D. P. Vercauteren; J. Catal. 2011**,** 281 (2), 212-221.
[123] A. A. Rybakov, A. V. Larin, G. M. Zhidomirov, D. N. Trubnikov, D. P. Vercauteren; Comp. Theor. Chem. 2011**,** 964 (1-3), 108-115.
[124] D. F. Plant, G. Maurin, I. Deroche, L. Gaberova, P. L. Llewellyn; Chem. Phys. Lett. 2006**,** 426 (4-6), 387-392.
[125] D. S. Wragg, R. E. Johnsen, M. Balasundaram, P. Norby, H. Fjellvåg, A. Grønvold, T. Fuglerud, J. Hafizovic, Ø. B. Vistad, D. Akporiaye; J. Catal. 2009**,** 268 (2), 290-296.

[126] I. Deroche, G. Maurin, P. L. Llewellyn, M. Castro, P. A. Wright; Microporous Mesoporous Mater. 2008**,** 107 (3), 268-275.
[127] D. F. Shantz, R. F. Lobo, C. Fild, H. Koller; Studies in Surface Science and Catalysis. Elsevier: 2000; Vol. 130, 845-850.
[128] M. J. Sabater, G. Sastre; Chem. Mater. 2001**,** 13 (12), 4520-4526.
[129] M. Haouas, E. Eilersten, K. P. Lillerud, F. Taulelle; "Unpublished results".
[130] J. i. Dědeček, S. Sklenak, C. Li, B. Wichterlová, V. Gábová, J. i. Brus, M. Sierka, J. Sauer; J. Phys. Chem. C 2009**,** 113 (4), 1447-1458.
[131] K. P. Schröder , J. Sauer; J. Phys. Chem. 1993**,** 97 (25), 6579-6581.
[132] C. Lo, B. L. Trout; J. Catal. 2004**,** 227 (1), 77-89.
[133] D. Zhou, Y. Bao, M. Yang, N. He, G. Yang; J. Mol. Catal. A: Chem. 2006**,** 244 (1–2), 11-19.
[134] D. W. Lewis, G. Sastre; Chem. Commun. 1999**,** (4), 349-350.
[135] M. Briend, M. J. Peltre, P. Massiani, P. P. Man, R. Vomscheid, M. Derewinski, D. Barthomeuf; Studies in Surface Science and Catalysis. Elsevier: 1994; Vol. 84, 613-620.
[136] M. E. Franke, U. Simon; Solid State Ionics 1999**,** 118 (3-4), 311-316.
[137] J. Sauer, C. M. Kölmel, J. R. Hill, R. Ahlrichs; Chem. Phys. Lett. 1989**,** 164 (2-3), 193-198.
[138] M. Sierka, J. Sauer; J. Phys. Chem. B 2001**,** 105 (8), 1603-1613.
[139] M. E. Franke, M. Sierka, U. Simon, J. Sauer; PCCP 2002**,** 4 (20), 5207-5216.
[140] G. Sastre, V. Fornes, A. Corma; J. Phys. Chem. B 2001**,** 106 (3), 701-708.
[141] B. P. C. Hereijgers, F. Bleken, M. H. Nilsen, S. Svelle, K. P. Lillerud, M. Bjørgen, B. M. Weckhuysen, U. Olsbye; J. Catal. 2009**,** 264 (1), 77-87.
[142] V. Kapko, C. Dawson, M. M. J. Treacy, M. F. Thorpe; PCCP 2010**,** 12 (30), 8531-8541.
[143] A. Sartbaeva, S. A. Wells, M. M. J. Treacy, M. F. Thorpe; Nature Mater. 2006**,** 5 (12), 962-965.
[144] K. A. Jackson; Kinetic Processes: Crystal Growth, Diffusion, and Phase Transitions in Materials. John Wiley & Sons: 2010.
[145] S. Stølen, T. Grande; Chemical thermodynamics of materials: macroscopic and microscopic aspects. John Wiley: 2004.
[146] E. A. Eilertsen, M. Haouas, A. B. Pinar, N. D. Hould, R. F. Lobo, K. P. Lillerud, F. Taulelle; Chem. Mater. 2012**,** 24 (3), 571-578.
[147] S. Malola, S. Svelle, F. L. Bleken, O. Swang; Angew. Chem. Int. Ed. 2012**,** 51 (3), 652-655.

Appendix

Papers I-III
Manuscript I
Unpublished results I+II
Posters I-III

Paper

I

A computational study on heteroatom distribution in zeotype materials

Mahsa Zokaie, Unni Olsbye, Karl P.Lillerud and Ole Swang

Microporous and Mesoporous Materials, Volume 158, 1 August 2012, Pages 175-179

Paper

II

Stabilization of silicon islands in silicoaluminophosphates by proton redistribution

Mahsa Zokaie, Unni Olsbye, Karl Petter Lillerud and Ole Swang

J. Phys. Chem. C, 2012, 116 (13), pp 7255–7259

Paper

III

Unit cell expansion upon coke formation in a SAPO-34 catalyst: A combined experimental and computational study

Mahsa Zokaie, David Wragg, Arne Grønvold, Terje Fuglerud, Jasmina Hafizovic Cavka, Karl Petter Lillerud and Ole Swang

Microporous and Mesoporous Materials, Volume 165, 1 January 2013, Pages 1-5

Manuscript

I

Lumpy Gravy: Size Distribution of Silicon Islands in SAPO Materials Based on Atomistic Modeling

Mahsa Zokaie, Unni Olsbye, Karl Petter Lillerud and Ole Swang

Unpublished result

I

Analysis of ^{29}Si NMR spectra for varieties of shapes and sizes of silicon islands

Unpublished result

II

Synthesis and characterization of SAPO-34 using N,N,N trimethyl-1-adamantammonium as a template

Poster

I

CHA and SAPO-34: Lattice stability dependence on position of acid sites

Mahsa Zokaie, Ole Swang, Stian Svelle, Merete Hellner Nilsen, Unni Olsbye and Karl Petter Lillerud

ABC-6, 6th world congress on Catalysis by Acids and Bases (10-14 May 2009, Genova, Italy)

CHA and SAPO-34:

Lattice stability dependence on position of acid sites

Mahsa Zokaie*, Ole Swang, Stian Svelle, Merete Hellner Nilsen, Unni Olsbye and Karl Peter Lillerud

inGAP Centre for Research-Based Innovation/Center for Materials Science and Nanotechnology, Department of Chemistry, University of Oslo, P.O. Box 1033, Blindern, N-0315 Oslo, Norway
e-mail: mahsaz@kjemi.uio.no

1 Introduction

The acidity, catalytic performance and long term stability of SAPO-34 and CHA depends on the number and distribution of Si and Al atoms in in these two frameworks and comes from hydroxyl group that compensates charge balance in system.

Si distribution in SAPO-34 and Al distribution in its zeolite analogue (CHA) has been investigated by using shell model potential molecular mechanics.
To find out how the stability of the lattice depends on Al-Al distance in CHA and Si-Si distance in SAPO-34, 2 Al atoms in CHA and 2 Si atoms in SAPO-34 were located in different positions in the framework.

In SAPO-34 substitution of P by Si was assumed and negative charge of both frameworks after substitution was balanced in two ways, modeling as-synthesized and active catalyst.

2 CHA and SAPO-34 structure

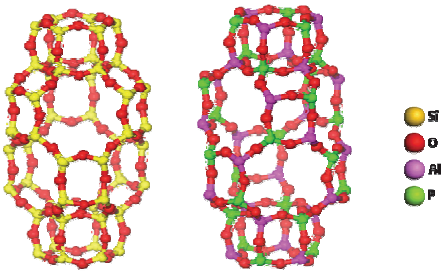

3 Distribution of Al in as-synthesized CHA and tested CHA .

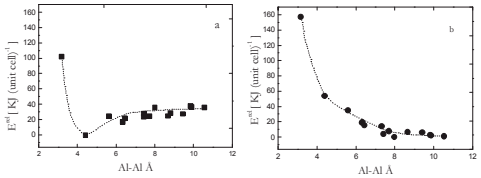

Relative energy as a function of the Al-Al distance in CHA calculated by GULP. The framework charge(-2 per hexagonal cell) is compensated a) by protonation (as-synthesized catalyst) b) by increasing all Si charges by 1/17 (Tested catalyst). (The dashed lines are just trend lines)

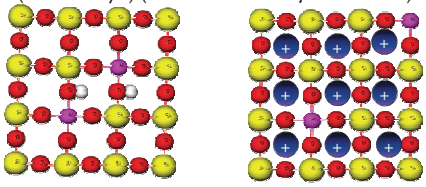

Illustration of most stable structures, left: as-synthesized CHA ,

right : tested CHA

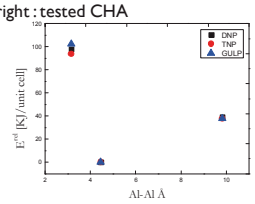

Comparison of DFT and GULP (protonation) for three random Al-Al distances.

4 Distribution of Si in as-synthesized SAPO-34 and tested SAPO-34.

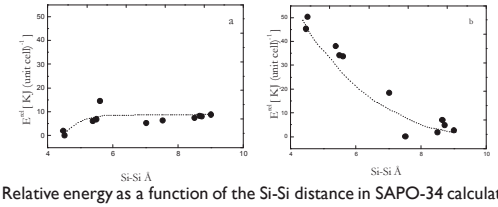

Relative energy as a function of the Si-Si distance in SAPO-34 calculated by GULP. The framework charge (-2 per super cell of 8 hexagonal cell) is compensated a) by protonation (as-synthesized catalyst) b) b) by increasing all Al and P charges by 1/144 and 1/142 respectively (Tested catalyst) (The dashed lines are just trend lines)

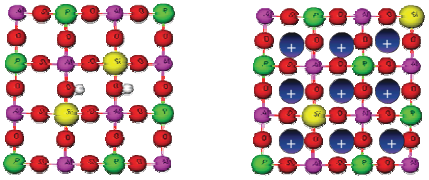

Illustration of most stable structures, left: as-synthesized SAPO-34 ,

right : tested SAPO-34

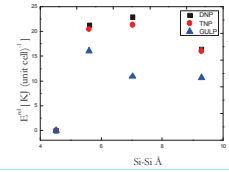

Comparison of DFT and GULP (protonation) for three random Si-Si distances.

5 Conclusion

CHA

- According to *Lowensteins' rule*, Al-O-Al linkages in zeolitic frameworks are forbidden and as we can see in figures (a ,b), this linkage gives least stable structure.
- For as-synthesized catalyst Al-O-Si-O-Al linkage gives most stable structure.
- For tested catalyst stability increases by increase of Al atoms distance.

SAPO-34 :

- For as-synthesized catalyst Si-O-Al-O-Si linkage gives most stable structure , but energy difference between most and least stable structure is about 10 KJ which is not very magnificent
- For tested catalyst stability increases by increase of Al atoms distance.

References

K.P.Schroder and Joachim Sauer, J.Phys. Chem, 1993,97,6579-6581
R.G.Bell et al. Zeolites, 1992, Vol 12, September/October
G. Sastre et al. J.Phys.Chem. 1996, 100, 6722-6730
G.Sastre et al. Journal of molecular catayasis A: Chemical 119(1997) 349-356

Poster

II

Silicon islands in SAPO materials: Thermodynamic considerations from atomistic modelling

Mahsa Zokaie, Merete Hellner Nilsen, Unni Olsbye, Karl Petter Lillerud and Ole Swang

16th International Zeolite Conference (4-9 July 2010, Sorrento, Italy)

Silicon Islands in SAPO Materials: Thermodynamic Considerations From Atomistic Modeling

Mahsa Zokaie, Merete Hellner Nilsen, Unni Olsbye, Ole Swang* and Karl Petter Lillerud *

inGAP Centre for Research-Based Innovation/Center for Materials Science and Nanotechnology, Department of Chemistry, University of Oslo, P.O. Box 1033, Blindern, N-0315 Oslo,Norway. e-mail: Ole.swang@kjemi.uio.no

Introduction

SAPO materials are crystalline, microporous silicoaluminophosphates in which silicon substitutes for some of the aluminum and phosphorus atoms in the framework. Substituting silicon for phosphorus in a neutral $AlPO_4$ framework introduces Brønsted acid sites that creates an active catalyst. A complicated feature of silicon incorporation in AlPOs is the formation of silicon islands. It has been found that heating of SAPO molecular sieves at high temperature (1100 K) induces a solid-state transformation due to the mobility of atoms and that isolated silicon atoms migrate to form silicon islands in the framework . In the present work, we apply the formalism of crystal nucleation to the description of silicon island formation.

Using analogy to solid $[SiO_2]$-liquid $[AlPO_4]$ phase system to study silicon island formation as a **nucleation** of a silica phase within the $AlPO_4$ structure:

Silicon island's free energy:

- Bulk energy G_v
- Surface energy γ

$$G = -4/3\pi r^3 G_v + 4\pi r^2 \gamma$$

By joining more silicon atoms to an island:

- Bulk energy increases as r^3
- Surface energy increases as r^2

Balance between bulk and surface energy at critical radii (r_c)

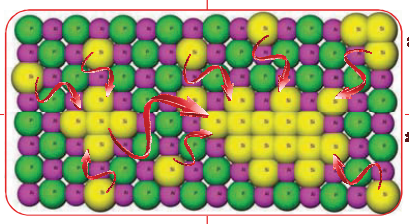

Critical radii :

- $\frac{\partial G}{\partial r} = 0$
- $r_c = \frac{2\gamma}{G_v}$

Silicon islands with radius smaller than r_c will be solvated, and the atoms will eventually merge into bigger islands.

Surface energy caused by interaction between silicon islands and the aluminophosphate famework .

Surface energy : $\gamma = \frac{(E_{AlPO-SiO_2} - 0.5E_{SiO_2} - 0.5E_{AlPO})}{A_{AlPO-SiO_2}}$

Models for calculating surface energy of the $AlPO_4$ / SiO_2 interface :

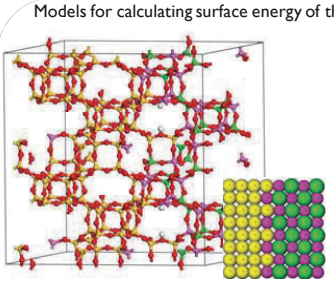

Vertical slab model

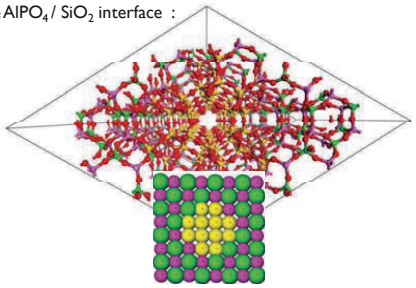

Cylinder model

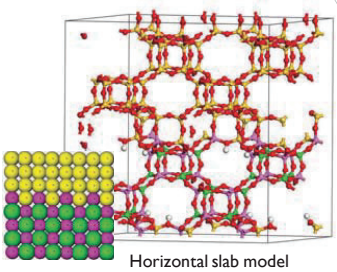

Horizontal slab model

The calculation of lattice energies and interfacial energies: at constant pressure using GULP code as implemented in Material Studio 4.4. forcefield : Catlow

Results and discussion

Model		Bulk energy (KJ/Å^3)	Surface energy (KJ/Å^2)	Critical radius Å
CHA	Cylinder model	-162.90	-643.53	7.9
	Horizontal slab model	-162.90	-624.66	7.7
	Vertical slab model	-162.90	-602.88	7.40
AFI	Cylinder model	-188.83	-749.58	7.9
	Horizontal slab model	-188.83	-695.07	7.4
	Vertical slab model	-188.83	-704.60	7.5

Table : Surface energy , bulk energy and critical radius for different models for SAPO-34(CHA) and SAPO-5(AFI)

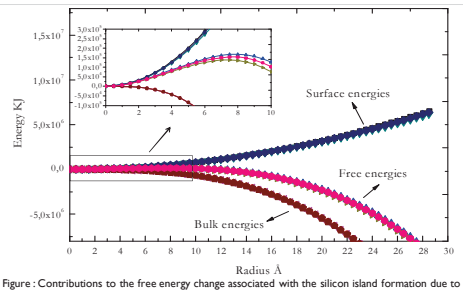

Figure : Contributions to the free energy change associated with the silicon island formation due to nucleation.

✓The critical radii of different models are very similar, in the range of 7.4 to 7.9 Å.

✓Comparison between critical radius of SAPO-34 and SAPO-5 shows no significant differences in critical radii of these two structures.

References

1.Wilson, S.T., R.W. Broach, C.S. Blackwell, C.A. Bateman, N.K. McGuire, and R.M. Kirchner, Microporous and Mesoporous Materials, 1999. **28**(1): p. 125-137.
2.Barger, P.T. and D.A. Lesch, Arabian Journal for Science and Engineering, 1996. **21**(2): p. 263-272.
3.Mertens, M., J.A. Martens, P.J. Grobet, P.A. Jacobs, D. Barthomeuf, E.G. Derouane, and W. Holderlich, NATO ASI Series B, 1990. **221**.
4.Sastre, G., D.W. Lewis, and C.R.A. Catlow, Journal of Molecular Catalysis A: Chemical, 1997. **119**(1-3): p. 349-356.
5.Derewinski, M., M.J. Peltre, M. Briend, D. Barthomeuf, and P.P. Man, Journal of the Chemical Society, Faraday Transactions, 1993. **89**(11): p. 1823-1828.
6.Ohring, M., *Engineering Materials Science.* 1995, San Diego: Academic Press.
7.Köhler, W. and S. Wiegand, *Thermal nonequilibrium phenomena in fluid mixtures* 2002, Berlin Springer.
8.Accelrys, *GULP* San Diego: Accelrys Software Inc. , http://www.accelrys.com.
9.Gale, J.D., J. Chem. Soc., Faraday T rans., 1997. **93**(4): p. 629-637.
10.Flanigen, E.M., R.L. Patton, and S.T. Wilson, *Studies in Surface Science and Catalysis*, W.J.M.E.F.V. P.J. Grobet and G. Schulz-Ekloff, Editors. 1988, Elsevier. p. 13-27.

Poster

III

Proton redistribution in silicon island of SAPO material

Mahsa Zokaie, Merete Hellner Nilsen, Unni Olsbye, Karl Petter Lillerud and Ole Swang

15th International FEZA Conference (3-7 July 2011, Valencia, Spain)

Proton Redistribution in Silicon Island of SAPO Material

Mahsa Zokaie[1], Merete Hellner Nilsen[1], Unni Olsbye[1], Karl Petter Lillerud *[1] and Ole Swang* [1,2]

1: inGAP Centre for Research-Based Innovation/Center for Materials Science and Nanotechnology, Department of Chemistry, University of Oslo, P.O. Box 1033, Blindern, N-0315 Oslo, Norway.
2: SINTEF Materials and Chemistry, P. O. Box 124, Blindern, N-0314 Oslo, Norway
e-mail: Ole.swang@kjemi.uio.no

Introduction

SAPO materials are crystalline, microporous silicoaluminophosphates in which silicon-proton pairs substitute for some of the aluminum and phosphorus atoms in the framework. An interesting feature of SAPOs is the formation of so-called «**silicon islands**», which are formed when at least two adjacent T sites are occupied by silicon.

The **preferred position of the proton** at isolated acid sites has been the subject of both experimental [1-4] and computational studies [5,6]. In a theoretical study of silicon island, it was assumed that the protons for keeping the silicon island neutral, would occupy the same positions as those preferred for solitary silicon atoms. [6-8]

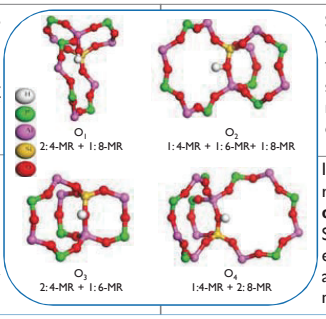

Figure 1: Four different crystallographic oxygen atoms in SAPO -34 structure (SAPO labeling scheme)

SAPO-34 has the highly symmetric Chabazite topology with only one symmetrically independent tetrahedral site (T-site) and **four unique oxygen sites**. The protons introduced to ensure charge neutrality after silicon inclusion may coordinate to one of the four different oxygens. (Figure 1)

In the present work, we have investigated the relative stabilities of **different proton distributions** around a 5-atom silicon island in SAPO-34 through periodic molecular mechanics energy minimization calculations [9] and we arrive at a number of criteria that a proton distribution must satisfy to be stable.

Silicon island models

- Model : SAPO-34 with island of 5 silicon atoms.
- Three protons to neutralize the charge of silicon island.
- No proton bonded to central silicon's associated oxygen atoms.

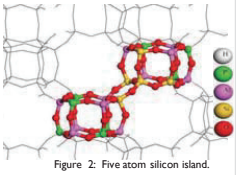

Figure 2: Five atom silicon island.

- Each tetrahedron will accommodate only one proton.

➲ **108** different structures, only differing in the proton positions.

Results and discussion

- Relative energy deviation in the data set is as high as 90 kJ/mol.
- Proton placement is critical for stability.
- No correlation between stability and electrostatic repulsion between the three protons based on their mutual positions.

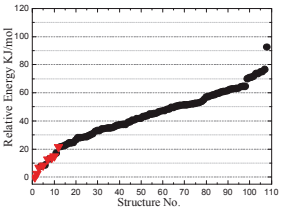

Figure 3: Relative energy of different structures calculated by molecular mechanics.

➲ Careful analysis of the different structures yielded **four criteria** for excluding structures as unstable.

Categories of unstable structures

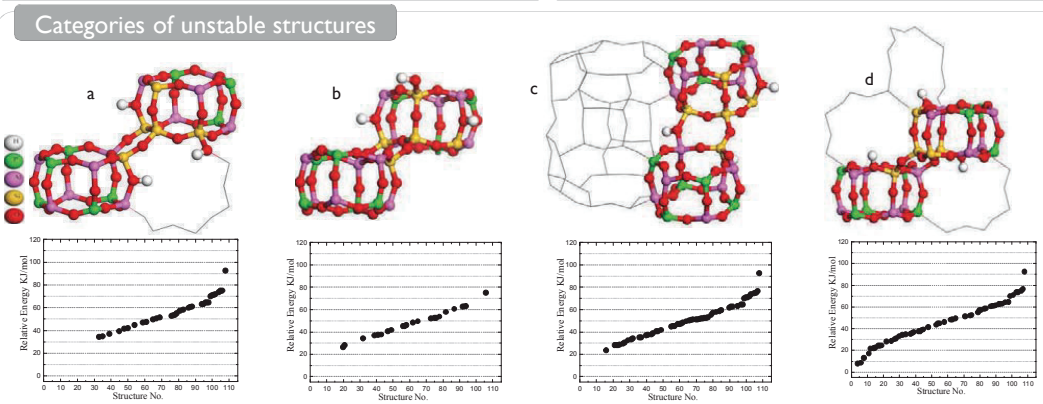

Figure 4 : Categories of unstable structures and the relative energies of their associated structures due to: a)Protons connected to oxygen atoms in the same ring, b)Protons connected to tetrahedra located in the same double six ring, c)Proton pointing to open space (connected to O_4) and d)Proton connected to O_2 .

Conclusion

➲ Calculation shows that the most stable configurations of protons around a silicon island cannot be predicted from the most-stable proton coordination for a single silicon atom.
➲ We have established criteria of stability for the proton configuration around a 5-atom silicon island in SAPO-34.
➲ The finding can be used to estimate the stable structure of larger islands.

References

[1] L. Regli, S. Bordiga, A. Zecchina, M. Bjørgen, K.P. Lillerud and C.C.a.S.C. Aldo Gamba, Studies in Surface Science and Catalysis, 155 (2005), 471-479
[2] S. Bordiga, L. Regli, D. Cocina, C. Lamberti, M. Bjørgen and K.P. Lillerud The Journal of Physical Chemistry B, 109 (2005), 2779-2784
[3] G.A.V. Martins, G. Berlier, S. Coluccia, H.O. Pastore, G.B. Superti, G. Gatti and L. Marchese, The Journal of Physical Chemistry C, 111 (2006), 330-339
[4] L. Smith, A.K. Cheetham, L. Marchese, J.M. Thomas, P.A. Wright, J. Chen and E. Gianotti Catalysis Letters, 41 (1996), 13-16
[5] R. Shah, J. D. Gale and M. C. Payne, Chemical Communications, (1997), 131-132
[6] G. Sastre and D.W. Lewis, Journal of the Chemical Society, Faraday Transactions, 94 (1998), 3049-3058
[7] A. Buchholz, W. Wang, M. Xu, A. Arnold and M. Hunger, Microporous and Mesoporous Materials, 56 (2002), 267-278
[8] M. Derewinski, M.J. Peltre, M. Briend, D. Barthomeuf and P.P. Man , Journal of the Chemical Society, Faraday Transactions, 89 (1993), 1823-1828
[9] Optimizations were carried out at constant pressure using the GULP code (Gale, J.D., Journal of the Chemical Society, Faraday Transactions, 1997, **93**(4): p. 629-637.) as implemented in Accelrys Materials Studio 4.5 (Accelrys Software Inc. , http://www.accelrys.com) The shell model potential forcefield of Catlow was used throughout (K.-P. Schröder, J. Sauer, M. Leslie, C. Richard, A. Catlow and J.M. Thomas, Chemical Physics Letters, 188 (1992) 320.)